# UTILIZING NANOTECHNOLOGY FOR DISEASE SEVERITY ASSESSMENT AND DRUG DELVERY IN CHRONIC OBSTRUCTIVE PULMONARY DISEASE

by

Jane Chisholm

A dissertation submitted to the Johns Hopkins University in conformance with the requirements for the degree of Doctor of Philosophy

Baltimore, Maryland

October, 2017

## Abstract

Chronic obstructive pulmonary disease (COPD) is currently the third leading cause of death in the United States with continuously elevating morbidity and mortality. COPD is a complex progressive disease primarily caused by cigarette smoke (CS) as well as other inhaled pollutants. The disease is characterized by chronic, irreversible obstruction of airflow from the lung, which is resulted from both airspace enlargement (i.e. emphysema), as well as airway inflammation, remodeling, and mucus hypersecretion (chronic bronchitis).

Perturbations in the properties of airway mucus contribute to accelerated lung function decline in patients with COPD, which leads to reduced quality of life and an elevated mortality rate. Alterations in the bulk physicochemical properties of mucus have been widely investigated in an attempt to unravel key factors affecting disease severity. Nonetheless, microstructural characteristics of mucus have not yet been explored in COPD. I first investigated whether the mesh size of spontaneously expectorated COPD sputum, as indicated by muco-inert nanoparticle diffusion, correlated with impaired lung function and altered sputum composition. I found that the diffusion of 100 nm muco-inert nanoparticles could sensitively differentiate microstructural features of sputum samples from cigarette smokers without airway obstruction and COPD patients. Nanoparticle mobility correlated with measurements of lung function as well as sputum solids and mucin content. These findings suggest that sputum microstructure as quantified by muco-inert nanoparticle diffusion may serve as a novel indicator and/or risk factor for COPD severity and progression.

There is currently no cure for COPD. Treatment options are limited to symptom relief and do not arrest or reverse the deterioration in lung function and architecture that accompanies the disease. Elevated transforming growth factor beta (TGF-β) signaling is strongly implicated as a key contributor to COPD development and progression. We have previously shown that an orally administered angiotensin receptor blocker (ARB) protected against airspace damage in animal models of COPD via TGF-β antagonism. Here I engineered an inhalable drug nanocrystal (NC) formulation based the ARB telmisartan (TEL; TEL-NC) for the localized treatment of COPD. The TEL-NC possess a bio-inert surface coating that promoted colloidal stability and minimized macrophage uptake, and thus, improved the local drug concentration following inhalation compared to both inhaled and orally administered free drug. I then investigated the efficacy of inhaled TEL-NC in two widely explored animal models relevant to COPD. Treatment with TEL-NC provided a protective effect in an acute cigarette smoke (CS)-induced injury model via suppression of TGF-β signaling and attenuation of oxidative stress and inflammation. In the tight-skin (TSK) transgenic emphysema model, inhaled TEL-NC provided therapeutic resolution of disease pathogenesis, while orally administered free drug had no therapeutic effect. These findings suggest that inhaled TEL-NC can prevent and/or reverse COPD-related disease manifestation caused by enhanced TGF-β signaling.

Advisor: Justin Hanes, Ph.D.

Thesis Committee: Justin Hanes, Ph.D., Rangaramanujam Kannan, Ph.D., Honggang Cui, Ph.D., Enid Neptune, M.D., and Jung Soo Suk, Ph.D.

## Acknowledgements

The work presented in this thesis would not have been possible without the guidance, support, and collaboration of many people. First and foremost I would like to thank my advisor, Dr. Justin Hanes, for giving me the opportunity to join his lab and work in the Center for Nanomedicine. I greatly appreciate that Dr. Hanes always emphasized "the big picture" and being aware of the clinical implications of our work. I would like to thank Dr. Jung Soo Suk for being an advisor and guiding me throughout my entire graduate school journey. I would also like to thank Dr. Laura Ensign for being a a wonderful friend and mentor.

I would like to thank my primary collaborator, Dr. Enid Neptune, for all of her help and support during my PhD. Dr. Neptune's enthusiasm for my work was infectious and helped me remain positive during the difficult times. Collaboration between physicians and engineers/researchers is critical to successful biomedical research and we are very privileged at Hopkins to be able to work with world class physicians who are experts in their fields, such as Dr. Neptune. I also need to thank the members of her lab Dustin Dikeman, Alla Malinina, and Armando Lopez-Mercado for all of their help. I would also like to thank all of the members of my thesis committee, Dr. Rangaramanujam Kannan and Dr. Honggang Cui, for agreeing to serve on my committee and providing valuable feedback on my dissertation.

During my many years in the CNM I have had the privilege to meet, work with, and befriend so many people that have all had an impact on me. I value all of my CNM relationships and I cannot adequately express in words what this experience and these people have meant to me. The unique collaborative structure of the CNM fosters a

wonderful diverse community environment. First I need to thank all of the current and past members of “The Lung Team” for their support, assistance, discussions, and friendship including Ben Tang, Nick Boylan, Anthony Kim, Ben Schuster, Gregg Duncan, Xinglu Huang, Namho Kim, and Jason Rodriguez. I specifically need to acknowledge one of the original members, Craig Schneider, who inspired me to pursue a Ph.D. and taught me everything I know about pulmonary drug delivery. Without Craig’s mentorship, support and friendship I would not be where I am today. Additionally, I must thank Julie Shade who was not only a superb undergrad but became a good friend. I was constantly impressed by her work ethic and scientific inquiry. I’m very proud of her and look forward to her future success as she pursues a Ph.D. of her own.

I especially need to recognize Elizabeth Nance and Clark Zhang for being my rocks during my Ph.D. I honestly do not think I could have survived this journey without their support, friendship and mentorship. I also would like to thank my classmate and friend Katharina Maisel who was always there for me inside and outside the lab and never failed to be a source of encouragement even in my darkest of days. I have to thank the “CNM Chicks,” including Taarika Babu, Thuy Hoang, Elga Bandiera, Mart Roig Pons, Hannah Zierden, Divya Rao, and Karina Negron. It is rare to have so many women together in a lab let alone ones who support each other and I am so grateful that I had the opportunity to work with and become friends with all of you.

I have to say a special thanks to our current and former administrators including Nicole Turner and Fareeha Zulfiqar and especially Joseph Vargas. It is because of you that the CNM runs smoothly and I greatly appreciate all of the work you do. There are many other past and present members of the CNM who have greatly impacted and

supported me during my graduate studies that I need to acknowledge including, Abhijit Date, Tao Yu, Kunal Parikh, Jairo Ortiz, Panos Mastorakos, Ting Shih, Ming Yang, Qinqquo Xu Jie Fu, Yoo Chun Kim, Matt Shin, Aditya Josyula, Siva Kambhampati, Fan Zhang, Josh Portfield, Kevin Liaw, Anjali Sharma, Rishi Sharma, Manoj Mishra.

Last but not least I have to thank my family and friends for being so supportive and understanding throughout this entire crazy journey. You all were always there for me and believed in me especially when I was most discouraged. I am particularly grateful for their patience when I had no answer to their question of when I will finally graduate. I am very lucky to have formed wonderful friendships in Baltimore outside of Hopkins that were a wonderful source of support and distraction. I especially want to thank my parents for their unwavering love and always encouraging and allowing me to pursue my own ambitions. I want to thank my brother and sister for their constant love, support and laughter. During the second year of PhD, my dad and my brother both were diagnosed with and subsequently survived serious medical conditions. This was a very trying time for me, especially since I was not close to home. However, their strong will, fight, positive attitude was inspirational and a constant reminder of the implications of my research. It is all too easy as researchers to get bogged down by the trivial details and lose perspective. It is important to step back every so often and be reminded of the ultimate goal. This thesis is dedicated to my dad and my brother.

## Table of Contents

## List of Figures

## List of Tables

# 1. Introduction

Chronic obstructive pulmonary disease (COPD) is currently the third leading cause of death in the United States with continuously elevating morbidity and mortality. COPD is a complex progressive disease primarily caused by cigarette smoke (CS) as well as other inhaled pollutants. The disease is characterized by chronic, irreversible obstruction of airflow from the lung, which is resulted from both airspace enlargement (i.e. emphysema), as well as airway inflammation, remodeling, and mucus hypersecretion (chronic bronchitis).

Mucus hypersecretion is a hallmark of COPD and contributes to the accelerated lung function decline, reduced quality of life, and mortality in COPD. While alterations in the bulk physicochemical properties of mucus have been investigated, microstructural characteristics of mucus that punctuate COPD disease progression have not yet been explored. In Chapter 3, I employed muco-inert nanoparticles to probe the sputum (expectorated mucus) from cigarette smokers without airway obstruction and patients with COPD. I investigated whether the mesh size of spontaneously expectorated sputum, as indicated by the muco-inert nanoparticle diffusion, correlated with impaired lung function and altered sputum composition.

There is no cure for COPD and the current standard of care is limited to relieving symptoms relief and improving quality of life. Elevated transforming growth factor beta (TGF-β) signaling is strongly implicated as a key contributor to COPD development and progression. We have previously shown that an orally administered angiotensin receptor blocker (ARB) protected against airspace damage in animal models of COPD via TGF-β antagonism. In Chapter 4, I engineered an inhalable drug nanocrystal (NC) formulation

based the ARB telmisartan (TEL; TEL-NC) for the localized treatment of COPD. In Chapter 5, I then investigated the efficacy of the inhaled TEL-NC formulation in two widely explored animal models relevant to COPD.

# 2. Background

## *2.1 Chronic obstructive pulmonary disease*

Chronic obstructive pulmonary disease (COPD) is currently the third leading cause of death in the United States with continuously elevating morbidity and mortality [1]. Of the six leading causes of death in the U.S., it is the only one whose mortality is increasing [2]. Thus COPD poses a large burden and is a major public health concern. COPD is a complex progressive disease primarily caused by cigarette smoke (CS) as well as other inhaled pollutants [3]. The disease is characterized by chronic, irreversible obstruction of airflow from the lung, which is resulted from both airspace enlargement (i.e. emphysema), as well as airway inflammation, remodeling, and mucus hypersecretion (chronic bronchitis) [4]. The relative contributions of airspace destruction and airway disease vary from person to person adding a level of complexity to the disease.

Common symptoms of COPD are dyspnea (i.e. breathlessness), chronic cough, and sputum production [4]. Spirometry is used to diagnose COPD and track lung function decline [5]. Specifically, airflow limitation (i.e. COPD) is defined as the ratio of the post-bronchodilator forced expiratory volume in one second ($FEV_1$) to the forced vital capacity (FVC) of 0.7 [4]. The $FEV_1$ measurement indicates lung function and a decrease in $FEV_1$ corresponds with lung function decline. Spirometry is a noninvasive and readily available test and is the most reproducible and objective measurement of airflow limitation [4]. The disease severity is classified based on the FEV1 percent predicted measured after inhalation of a short-acting bronchodilator and is classified into four stages by the Global Initiative for Chronic Obstructive Lung Disease (GOLD) known as GOLD stages shown in Table 2.1 [4]. Results from surveys such as the modified British

Medical Research Council (mMRC) Questionnaire [6], the Chronic Respiratory Questionnaire [7], the St. George's Respiratory Questionnaire (SGRQ) [8], and the COPD assessment test (CAT) also contribute to COPD symptom evaluation [4]. Since COPD is a heterogeneous disease that affects patients differently, a multidimensional assessment is necessary for diagnosis and assessment [9].

There is currently no cure for COPD. Treatment options are limited to relieving symptoms, reducing frequency and severity of exacerbations, and improving quality of life. No therapies arrest or reverse the deterioration in lung function and architecture that accompanies the disease [10]. Smoking cessation influences the nature history of disease and is the most effective way to limit disease progression [11]. The primary pharmacological treatments for COPD are inhaled bronchodilators and corticosteroids [4, 12]. Bronchodilators dilate the small airways which allows for increased airflow to the lungs and reduced dyspnea [13]. There are two main classes of bronchodilators, $\beta_2$-agonists and anti-muscarinics [13]. $\beta_2$-agonists function by binding to $\beta_2$-adrenergic receptors which stimulates smooth muscle relaxation, and there are both short-acting and long-acting $\beta_2$-agonists (SABAs and LABAs, respectively) [4]. Anti-muscarinics prevent bronchoconstriction and mucus secretion via antagonism of muscarinic receptors. There are also short-and long-acting antimuscarinics (SAMAs and LAMAs, respectively) [4]. Often these medications are given in combination. Inhaled corticosteroids (ICS) are typically used in combination with LABAs in patients with severe COPD and exacerbations. Besides pharmacological therapy, oxygen therapy and exercise programs are often implemented [4]. Surgery to remove the diseased tissue is considered a last resort [14].

## *2.2 Airway mucus*

Airway mucus functions as a selectively permeable barrier, allowing nutrients, proteins, and other molecules to move through it, while protecting the underlying epithelium by excluding inhaled pathogens and particulates [15-17]. Once trapped, foreign materials are rapidly cleared from the lungs via mucociliary clearance (MCC) where the mucus is subsequently swallowed [16]. A mucus layer ~ 1-10 μm thick is maintained by continuous secretion of mucus from goblet cells present in the airways and submucosal glands [18] and lines the luminal surface of the lungs from the trachea to the terminal bronchioles.

Airway mucus is a viscoelastic gel comprised of a complex mixture of mucins, cells, cellular debris, bacterial proteins, antibacterial products, and water [19]. The gel properties of mucus are produced mucins, which are large highly glycosylated proteins. The majority of the glycans on mucins are negatively charged imparting an overall negative charge to the mucin fibers. Mucins also contain cysteine rich domains where no glycosylation is present. These "naked" regions form into hydrophobic beads or globules that are stabilized by internal disulfide bonds [16]. Thus mucus can adhesively trap particulates due to both electrostatic and hydrophobic interactions. Further, the gel structure formed by the mucin network sterically traps particulates that are larger than the mucus pore size.

## *2.3 Mucus in COPD*

One cause of airflow obstruction in COPD is an accumulation of mucus in the airways. This facet of COPD is referred to as chronic bronchitis (CB) and is typically

defined as the presence of a chronic, productive cough and sputum production for at least 3 consecutive months in 2 consecutive years [20]. Sputum is mucus that is cleared via cough and expectorated from the mouth. Accumulation of mucus in COPD is due to both mucus overproduction and hypersecretion by goblet cells and submucosal glands [21, 22] as well as reduced clearance [23, 24], which results in luminal occlusion of airways [25]. The mucus hypersecretion in COPD has many causes including cigarette smoke exposure [26, 27], viral and bacterial infections [28, 29], and inflammation [29]. COPD patients with CB have an increased number of goblet cells and mucin stores [30]. Clinically, mucus hypersecretion and occlusion are associated with accelerated lung function decline [31], increased exacerbation and hospitalization rates [32], and increased mortality [33]. Many of the current treatments for COPD intervene in the physiological mechanisms of CB. For example, $\beta_2$-agonists increase ciliary beat frequency while anti-muscarinics and gluococorticoids reduce mucus secretion and production, respectively [20].

Alterations in the composition of mucus directly affect its biophysical properties, which can result in dysfunctional MCC and subsequent disease manifestations [34]. In COPD patients with CB, an enhanced expression of gel forming mucins and elevated overall sputum solids content is observed in the lumen of the small airways [21, 35]. The increased solids content in sputum samples from CB patients was found to correlate with elevated partial osmotic pressure of the mucus gel layer and impaired mucus clearance [36]. Furthermore, it was recently reported that the total mucin concentration was significantly higher in induced sputum from patients diagnosed with CB compared to those without CB [37]. Functional MCC is dependent on appropriate rheological properties of airway mucus [38]. Macro- (or bulk-) rheological measurements have

revealed an increased viscoelasticity of COPD sputum compared to mucus from healthy subjects [39], which is likely related to the elevated macromolecule concentration found in COPD sputum.

### *2.4 Pulmonary drug delivery*

Inhalation drug delivery is a non-invasive strategy for the delivery of drugs systemically or locally to the lungs. In particular, inhalational delivery of drugs directly to diseased tissue in the lung is attractive as it provides direct, topical delivery of the drug on site in the lungs while negating first pass metabolism and reducing the exposure of other tissues to the therapeutic [40-44]. Unfortunately, drugs inhaled directly to the lung are rapidly removed via systemic absorption and mucociliary clearance [45, 46], resulting in a very short time that the drug concentration remains in the therapeutic window. Frequent daily administration and the short duration of clinical effects are major disadvantageous of inhaled drug formulations [47, 48]. Additionally, due to the extensive vascularization of the lungs, most inhaled drugs enter the systemic circulation within minutes of administration, which may lead to off-target effects.

### *2.5 Nanoparticles for pulmonary drug delivery*

Pulmonary drug delivery via nanoparticles (NP) may address the shortcomings of conventional inhalational drug delivery by increasing the time the drug is in the therapeutic window and reducing systemic exposure directly following inhalation. Thus, this strategy can reduce the required dose, dosing frequency and systemic side effects. The advantages of locally administered nano-based systems can include, (i) sustained and

controlled release of drugs locally [49, 50], (ii) protection of cargo drugs against degradation or inactivation [51, 52], (iii) reduction of side effects by lowering total dose and dose frequency [53, 54], and (iv) potential to overcome a variety of extracellular and intracellular barriers due to nanometric size [55-59]. There are a variety of types carriers for lung delivery including nanoparticles, liposomes, dendrimers, and nanocrystals [47].

Specifically, biodegradable polymers are extensively used as the carrier to encapsulate therapeutics in nanoparticulates. Specifically, poly(lactic-co-glycolic acid) (PLGA), an FDA-approved material, is the most widely used biodegradable polymer for nanoparticulate drug delivery. PLGA is a versatile polymer and has been used to encapsulate a variety of small molecule drugs, proteins, and nucleic acids in particulate carriers [60]. *In vivo*, PLGA slowly bioerodes via hydrolysis of the ester backbone and breaks down into its monomeric components (lactic acid and glycolic acid) [61]. As these products are naturally occurring metabolites in the human body, PLGA is generally well tolerated *in vivo* for biomedical applications.

### *2.6 Mucus penetrating particles*

Mucus is the primary barrier to effective pulmonary delivery of therapeutic nanoparticles. We have previously shown that densely coating NP surfaces with polyethylene glycol (PEG) produces muco-inert particles (MIP), also known as mucus-penetrating particles (MPP), that are capable of moving in various human mucus secretions without being trapped by adhesive interactions with the mucus [62-65]. PEG is a hydrophilic and neutrally charged polymer thus surface PEGylation negates the electrostatic and hydrophobic interactions with mucus. The diffusion of MIP in mucus

can be slowed by steric obstruction imposed by the microstructure of the gel. In other words, MIP of a given size will move more slowly in a mucus sample with a tighter mesh, especially if the MIP diameter approaches the average pore size of the mucus [62-65]. Conversely, conventional polymeric NP are trapped in mucus regardless of particle size due to adhesive interactions with mucus constituents; such particles are referred to as "conventional particles" (CP) or muco-adhesive particles (MAP). Thus, NP must be both smaller than the mucus mesh spacing and possess a dense surface coating of PEG in order to effectively diffuse in mucus.

The diffusion of variously sized MIP has previously been employed as a biophysical tool to probe the microstructure of human cervical vaginal [62], respiratory [64], and chronic rhinosinusitis mucus [65] and cystic fibrosis (CF) sputum [63, 66]. Multiple particle tracking (MPT) allows simultaneous tracking of hundreds of individual particles in highly complex and heterogeneous biological specimens at high spatiotemporal resolution and quantification of individual particle transport rates [67]. MPT is a powerful and versatile technique. Specifically, using this technology we have found that MIP as large as 200 nm are capable of rapidly diffusing in respiratory mucus collected from endotracheal tubes [64]. We also determined the average pore size of sputum from patients with CF to be ~140 ± 50 nm [63]. Further, we demonstrated that the addition of a mucolytic to CF sputum improved the diffusion of MIP indicating an increase in the microstructure [66, 68].

This information can also be applied to design drug and gene carriers for inhaled delivery to potentially improve the efficacy of the therapeutic compared with conventional nanoparticles or free drug formulations [69]. Pulmonary delivery of various

types of MIP including polystyrene [70], biodegradable [70], and non-viral gene vectors [71, 72] exhibited improved distribution in mouse lung airways and airspace compared to their unPEGylated counterparts. Importantly, the MIP formulations were retained in the lungs longer than the MAP [70-72]. The improved distribution and retention translated to improved efficacy in an acute model of lung inflammation of dexamethasone phosphate loaded PLGA NP [70] and also enhanced transgene expression in the lungs [71, 72].

### *2.7 Drug Nanocrystals*

Drug nanocrystals (NC) or nanosuspenions (NS) have become a widely used strategy to address the limitations of poorly water soluble drugs [73, 74]. Drug NC are particulates that are less than 1 micron and consist solely of the drug and a surfactant for stabilization. The nanonization process increases the surface area to volume ratio which increases the solubility and dissolution rate thereby improving the drug bioavailability and pharmacokinetics [75]. The two primary methods used to produce NC are either bottom up where the drug is precipitated or top down where mechanical force such as media milling or homogenization physically breaks apart the large insoluble particulates [73, 74]. However, only the top down approaches are currently used in the production of commercial products [76]. Drug NC have many advantages including, high efficiency of drug loading, feasibility for scale up, and applicability to a variety of administration routes [74]. The simplicity of the composition and the well-established industrial practice also result in lower regulatory barriers for the development of NS products. There are currently multiple NC formulations approved for clinical use and many more in preclinical development [73, 77].

We have previously developed a mucus penetrating NC formulation with curcumin (CUR) composed solely of the drug and Pluronic F127 [78]. Pluronics are triblock copolymer surfactants composed of hydrophobic polypropylene oxide (PPO) flanked by two hydrophilic polyethylene oxide (PEO, aka PEG) arm segments. The hydrophobic PPO core group can adsorb onto hydrophobic surface of nanoparticle surfaces, while the PEG chains form a hydrophilic and neutral shell that can shield the particle surface from interactions with mucus [79]. Of the multiple Pluronics tested, the F127-coated CUR NC exhibited the highest diffusions rates in cystic fibrosis sputum. Interestingly, the ability to penetrate mucus was dependent on the PPO molecular weight as opposed to the PEG molecular weight. In vivo, inhaled F127 CUR NC exhibited improved coverage of the airway epithelium compared with the non-mucus penetrating F68 CUR NC and free CUR.

### *2.8 TGF-β pathway and COPD*

The transforming growth factor (TGF)-β superfamily consists of over 40 members that act as multifunctional regulators of cell growth and differentiation during organ development [80, 81]. Three TGF-β isoforms, including TGF-β1, β2 and β3, have been identified in the mammalian lungs and play distinct roles in lung development and repair [82]. These TGF-β isoforms all bind to the type II TGF-β receptor and mediate the recruitment of the type I receptor to form a heteromeric complex, thereby initiating a stereotyped series of cell-type specific responses in the lung airways (i.e. bronchi and bronchioles) and airspace (i.e. alveoli) [82]. TGF-β signaling is tightly controlled to maintain physiological homeostasis in the healthy lung [82]. Alterations in TGF-β

expression is associated with COPD development and progression, and elevated TGF-β levels have been shown in both the airway and airspace compartments of patients with COPD [83]. Further, in pre-clinical models, cigarette smoke exposure increases TGF-β signaling throughout the lung parenchyma, thereby triggering oxidative stress injury, inflammation, epithelial cell death and airway remodeling [84-88]. These processes likely culminate in the small airway obstruction and airspace destruction that are hallmarks of COPD.

### *2.9 COPD animal models*

There are a variety of COPD mouse models and these are typically classified as either acquired/induced or genetic models. The most commonly used induced models are generated by exposure to cigarette smoke (CS) [89-91]. This is logical given that the primary risk factor for COPD development and progression in humans is tobacco smoke. The COPD-like pathology is established by daily CS exposure for an extended period of time, typically weeks to months, either via whole body or nose-only exposure systems [90]. While nose-only systems allow for more direct control of the CS exposure compared with whole body exposure, they also require prolonged restraint of the animals. Further, the number of animals that can be exposed at a time is limited with the nose-only systems. Regardless of exposure modality, mice exposed to chronic CS develop airspace enlargement, small airway remodeling, chronic inflammation, and elevated oxidative stress [92]. However, the major limitation of smoke exposure models is that regardless of the model parameters, the pathology of severe disease in humans cannot be replicated [89]. Specifically, while CS exposure can produce the emphysema phenotype, mucus

hypersecretion and airway obstruction are not established despite the presence of goblet cell metaplasia and airway remodeling [92]. Thus, the typical CS exposure models may only be appropriate to evaluate therapeutics for emphysema as opposed to the chronic bronchitis phenotype. Additionally, there is little standardization of the CS-exposure model across labs [89, 91]. The mouse strain and type of cigarettes used can greatly impact the degree of disease produced.

Another acquired model is generated by inhalation of neutrophil or pancreatic elastase can also be used to induce emphysema and inflammation [89]. A major advantage of this model is that emphysema can be rapidly induced by only a single administration of elastase, compared with the CS-exposure model that can take six months to establish [91]. However, the mechanisms behind elastase emphysema are unclear and may not be as relevant to CS generated emphysema.

The COPD animal models based on genetic variations include natural mutant, transgenic and knockout models [93]. Compared with the acquired models of COPD, the genetic models offer consistency and assurance of disease development; however, they do not necessarily reflect the lung pathogenesis relevant to COPD in humans. Interestingly, there are several spontaneous mutants that manifest an emphysema phenotype [93]. One example is the tight skin (TSK) mouse which has a heterozygous mutation in fibrilin-1[94]. Fibrilin-1 is a glycoprotein that is involved extracellular matrix deposition during development and remodeling [95]. This mutation results in excess matrix deposition with fibrosis in the skin as well as impaired alveolar septation that evolves into progressive airspace enlargement [96, 97]. This phenotype is at least

partially attributed to cell death as a result of oxidative stress [98]. However, inflammation has not been implicated in the pathology [99].

**Table 2.1.** GOLD staging system for COPD severity

| GOLD Stage | COPD severity | FEV1/FVC ratio | FEV1 range |
|---|---|---|---|
| I | Mild | <0.07 | ≥80% of normal |
| II | Moderate | <0.07 | 50-79% of normal |
| III | Severe | <0.07 | 30-49% of normal |
| IV | Very severe | <0.07 | <30% of normal |

# 3. Nanoparticle diffusion in spontaneously expectorated sputum as a biophysical tool to probe disease severity in COPD

## *3.1 Introduction*

Mucus abnormalities contribute to chronic morbidity in a variety of lung diseases, including chronic obstructive pulmonary disease (COPD) [100, 101], cystic fibrosis (CF) [102], and asthma [103]. COPD is the third leading cause of death in the US [1], and at least 30% of people with COPD have chronic bronchitis (CB), characterized by chronic cough and sputum production [104, 105]. In healthy lungs, mucus that lines the luminal surface of lung airways serves a critical protective purpose by trapping inhaled particulates and pathogens that are subsequently cleared from the airways via mucociliary clearance (MCC) [17, 106]. However, in obstructive lung diseases, mucus hypersecretion can overwhelm mucus clearance mechanisms and result in bacterial overgrowth, chronic airway inflammation, and airway obstruction [107]. Specifically in COPD, mucus hypersecretion is associated with accelerated lung function decline [31], increased hospitalization rate, and increased mortality [32]. Mucus obstruction of the small airways may also be a significant predictive factor of COPD progression and mortality [25, 108], as well as exacerbation risk [109-111].

Airway mucus is a viscoelastic gel comprised of a complex mixture of high molecular weight mucin glycoproteins, cells, cellular debris, bacterial proteins, antibacterial products, and other molecules [19]. Alterations in the composition of mucus directly affect its biophysical properties, which can result in dysfunctional MCC and subsequent disease manifestations [34]. In COPD patients with CB, an enhanced

expression of gel forming mucins and elevated overall sputum solids content is observed in the lumen of the small airways [21, 35]. Recently, Anderson and colleagues found that increased solids content in sputum samples from CB patients correlated with elevated partial osmotic pressure of the mucus gel layer and impaired mucus clearance [36]. Functional MCC is dependent on appropriate rheological properties of airway mucus [38]. Macro- (or bulk-) rheological measurements have revealed an increased viscoelasticity of COPD sputum compared to mucus from healthy subjects [39], which is likely related to the elevated macromolecule concentration found in COPD sputum. However, conventional bulk rheology measurements do not reveal properties of mucus or sputum at the microscopic level, which significantly contribute to mucus physiology and may correlate with disease pathology [112].

The diffusion rate of variously sized nanoparticles has previously been employed as a biophysical tool to probe the microstructure of human mucus and sputum secretions [62-65], as well as other biological specimens, including the vitreous gel [113], brain extracellular matrix [114] and tumor tissues [115]. Compared to other methods such as fluorescence recovery after photobleaching (FRAP) that only provide ensemble-averaged diffusion rates, multiple particle tracking (MPT) allows simultaneous tracking of hundreds of individual particles in highly complex and heterogeneous biological specimens at high spatiotemporal resolution and quantification of individual particle transport rates [67]. We have previously shown that densely coating nanoparticle surfaces with polyethylene glycol (PEG) produces muco-inert nanoparticles (MIP), also known as mucus-penetrating particles (MPP), that are capable of moving in various human mucus secretions without being trapped by adhesive interactions with the mucus [62-65]. The

diffusion of MIP in mucus can be slowed by steric obstruction imposed by the microstructure of the gel. In other words, MIP of a given size will move more slowly in a mucus sample with a tighter mesh, especially if the MIP diameter approaches the average pore size of the mucus [62-65]. Conversely, conventional polymeric nanoparticles are trapped in mucus regardless of particle size due to adhesive interactions with mucus constituents; such particles are referred to as "conventional particles" (CP) or muco-adhesive particles (MAP).

In this pilot study, we characterized MIP diffusion in spontaneously expectorated sputum from a cohort of cigarette smokers with and without airway obstruction to assess whether the sputum microstructure that governs MIP transport is associated with COPD disease severity and airway obstruction**.** Using MPT we found that sputum microstructure, as measured by MIP diffusion rates, correlated inversely with COPD disease severity and positively with FEV1/FVC ratio. A significant correlation was also observed between sputum microstructure and percent solids content and DNA concentration, respectively. Some of the results of these studies have been previously reported in the form of an abstract [116].

## *3.2 Methods*

### *3.2.1 Collection of spontaneously expectorated sputum*

Subpopulations and Intermediate Outcomes in COPD Study (SPIROMICS) is a multi-center longitudinal, observational study to identify novel phenotypes and biomarkers of COPD [117]. Smokers (pack years ≥20 years) with or without airway obstruction were pre-stratified into three categories based on spirometric pulmonary

function measurements, specifically forced expiratory volume in 1 second ($FEV_1$) and forced vital capacity (FVC): cigarette smokers without airway obstruction (smoker, $FEV_1/FVC>0.70$, FVC>LLN), mild-moderate COPD (mCOPD, $FEV_1/FVC<0.70$, $FEV_1>50\%$), and severe COPD (sCOPD, $FEV_1/FVC<0.70$, $FEV_1<50\%$). For our study specifically, participants were asked to provide an expectorated sample if possible at the same time as one of their annual scheduled SPIROMICS visits before providing an induced sample. Participants rinsed their mouths with water and after a deep breath with slow exhalation used a coughing manoeuvre to produce a deep sputum sample. Samples were stored at 4°C and analyzed by MPT within 24 h of collection in order to minimize sample degradation [66]. Aliquots used to determine mucin and DNA content were frozen at -80°C until use.

### *3.2.2 PEGylation of PS particles*

Fluorescent, carboxylate-modified polystyrene particles (PSCOOH) ranging in size from 100-500 nm were purchased from Life Technologies (Carlsbad, CA). PEG-modified particles (PSPEG) ranging in size from 100-500 nm were prepared by covalently conjugating 5 kDa methoxy-PEG-amine (Creative PEGworks, Winston Salem, NC) to the carboxyl groups on PSCOOH using carbodiimide coupling chemistry, as previously described [114]. Particle hydrodynamic diameter, polydispersity index (PDI), and surface charge (ζ-potential) were measured by dynamic light scattering (DLS) and laser Doppler anemometry with a Malvern Zetasizer Nano ZS (Malvern Instruments) in 10 mM NaCl, pH 7.4 and 25ºC, as previously described [63, 64].

### *3.2.3 Multiple particle tracking*

MAP and MIP diffusion in sputum was measured by MPT, as previously described [67, 118]. Sputum aliquots (~30 μl) were taken out of the sputum sample using a Wiretrol (Drummond Scientific Company, Broomall, PA) and placed in custom microscopy chambers. Diluted nanoparticle suspensions were added to the sputum at a final dilution of ~3% v/v. A 0.5 μl aliquot of green fluorescent PSCOOH plus 0.5 μl of red fluorescent PSPEG particles for each particle size (100, 200, and 500 nm) were added to each chamber. The samples were gently stirred and the chambers were sealed with a coverslip to prevent sample dehydration and equilibrated for 30 minutes before imaging. The chambers were imaged at room temperature using an inverted epifluorescence microscope (Axio Observer; Zeiss, Germany) on a vibration table with a 100x/1.46 NA oil-immersion objective. Movies were recorded for 20 s at a temporal resolution of 67 ms using an EM-CCD camera (Evolve 512; Photometrics, Tuscan, AZ).

Movies were analyzed with a custom automated particle tracking software in MATLAB (Mathworks; Natick, MA) to extract the *x* and *y* positions of particle centroids over time [67, 119]. At least 100 particles of each size and type were tracked for a minimum of 50 frames. The time-averaged mean squared displacement (MSD) as a function of time scale, τ, was calculated for each particle trajectory as:

$$\langle \Delta r^2(\tau) \rangle = \langle [x(t+\tau) - x(t)]^2 \rangle + \langle [y(t+\tau) - y(t)]^2 \rangle$$

Sputum samples were assumed to be locally isotropic (although not homogenous), thus the 2D MSD measured can be extrapolated to 3D MSD [120]. Median MSD values were reported for each sample instead of the ensemble average due to the inherent heterogeneity, and non-normal distribution of muco-inert nanoparticle (MIP) diffusion in

COPD sputum [121]. Previously we showed that the estimated static error is much smaller than the particle displacements, therefore static error is not expected to significantly impact the calculated MSD [122]. Additionally, we previously found that the effect of static and dynamic error in MPT experiments was minimized for MSD measured at $\tau = 1$ s ($MSD_{1s}$). Thus, median $\log_{10}MSD_{1s}$ was used as our primary measurement readout [67, 119, 122].

### *3.2.4 Quantification of sputum components*

The total solids content of sputum was determined by freeze-drying. Sputum sample aliquots of known mass were frozen in liquid $N_2$ and lyophilized (Labconco, Kansas City, MO) for at least 12 hours to remove water from the samples. The sputum solid content is calculated as the ratio of dry mass to wet mass.

Mucin concentration was determined based on the reaction of 2-cyanoacetamide (Sigma-Aldrich) with O-linked glycoproteins, as previously described [123, 124]. Sputum aliquots were diluted 20-fold and homogenized by vortexing for at least 15 minutes. Then, 50 µl of the suspension was reacted with 60 µl of an alkaline solution of 2-cyanoacetamide (200 µl of 0.6 M 2-cyanoacetamide mixed with 1 ml of 0.15 M NaOH) at 100ºC for 30 min. After incubation, 0.5 ml of 0.6 M borate buffer, pH 8.0, was added and the fluorescence intensity was measured at excitation and emission wavelengths of 336 and 383 nm, respectively. Sputum mucin concentrations were calculated with reference to a standard curve generated using known concentrations of mucin from bovine submaxillary gland (Sigma-Aldrich).

DNA concentration was measured using a fluorimetric assay based on the reaction of diaminobenzoic acid (DABA; Sigma-Aldrich) with DNA, as previously described [123]. Sputum aliquots were diluted 5-fold and homogenized by vortexing for at least 15 min. Next, 30 µl of this suspension was mixed with 30 µl of 20% w/v DABA solution and incubated at 60°C for 1 h. One ml of 1.76 M HCl was then added to stop the reaction. The fluorescence was measured at excitation and emission wavelengths of 390 and 530 nm, respectively. Sputum DNA concentrations were calculated based on a standard curve generated using known concentrations of DNA from salmon testes (Sigma-Aldrich).

### *3.2.5 Statistics*

Statistical significance was determined via a two-tailed Student's t test, assuming unequal variances. Comparisons between multiple groups were determined using one-way analysis of variance (ANOVA) with Tukey's post hoc test. Calculations were performed using GraphPad Prism software. P values less than 0.05 were considered significant.

## *3.3 Results*

### *3.3.1 Participant characteristics*

Demographic data was available on 36 participants: 9 smokers, 19 with mild-moderate COPD (mCOPD), and 8 with moderate-severe COPD (sCOPD) (Table 3.1). The transport analysis based on particle surface property and nanoparticle size was performed on samples from 18 participants (5 smokers, 7 mCOPD, 6 sCOPD) (Table 3.2). An additional 18 samples (4 smokers, 12 mCOPD, 2 sCOPD) were collected for the microstructure correlations between the biochemical composition and the lung function parameters; however, not all data was available for all patients.

### *3.3.2 Transport of nanoparticles in spontaneously expectorated sputum from smokers without airway obstruction*

Nanoparticle movement in mucus approximates both the mesh "tightness" and the pore size within the mucus gel [66]. To establish whether differences in particle diameter and mucus adhesivity affected particle movement in sputum from smokers, we first compared the transport behavior of MIP to that of similar sized MAP in spontaneously expectorated sputum samples from cigarette smokers without airway obstruction (n = 5). The dense PEG coating on the MIP resulted in an increased particle diameter and more neutral surface charge as measured by the ζ-potential (Table 3.3). For simplicity, hereafter we refer to nanoparticles based on their nominal size as reported in Table 3.3. We found that MAP, regardless of particle diameter, did not move rapidly through the sputum samples, as evidenced by their highly confined trajectories (Figure 3.1A, top). In contrast, 100 nm MIP moved through the sputum samples readily (Movie E1), as

evidenced by their diffusive trajectories (Figure 3.1A, bottom). We further quantified diffusion rates of each particle type, as parameterized by the median MSD. MSD represents the distance traveled by an individual particle in a given time interval (i.e. time scale) and, thus, MSD linearly correlates with particle diffusion rates. Although we observed that 300 nm MIP appeared to move more freely in sputum than 300 nm MAP, only the 100 nm particles displayed a statistically significant difference in MSD between the MIP and MAP at a time scale of 1 s (Figure 3.1B; $p < 0.05$). Further, both the 500 nm MIP and MAP moved exceedingly slowly in sputum, and the difference in MSD between 500 nm MIP and MAP was not significant.

### *3.3.3 Transport of nanoparticles in spontaneously expectorated sputum from patients with COPD*

We next compared the diffusion of MAP and MIP in sputum samples collected from patients with COPD (n = 13; Movie E2, 100 nm MIP). The 100 and 300 nm MIP exhibited more diffusive trajectories as compared to those of similar sized MAP (Figure 3.2A). Quantitatively, the MSD of 100 and 300 nm MIP were significantly greater than that of the MAP counterparts (Figure 3.2B, $p<0.05$). Similar to the observation in smoker sputum, 500 nm MIP and MAP were both trapped in COPD sputum: 500 nm MIP were trapped because they are too large to move through the pores (Movie E3); 500 nm MAP were trapped because they are likely both too large and adhesive to the sputum mesh elements.

### *3.3.4 Transport of MIP in sputum samples from smokers without airway obstruction, with mild-moderate COPD, and with severe COPD*

Diffusion of individual 100 and 300 nm MIP in smoker sputum samples exhibited unimodally higher diffusion rates compared with mCOPD and sCOPD samples, as quantified by particle $\log_{10}[MSD_{1s}]$ (Figure 3.3A and 3.3B, top panel). In contrast, particle transport was more obstructed in mCOPD and sCOPD sputum samples, as evidenced by the leftward shift of the MSD distribution and the reduced fraction of rapidly diffusing nanoparticles (Figure 3.3A and 3.3B, middle and bottom panels). In particular, the distribution of individual particle $\log_{10}[MSD_{1s}]$ in sCOPD was multi-modal with a larger fraction of slow-moving particles (Figure 3.3A and 3.3B, bottom panel). Specifically, this trend was most pronounced when comparing the 100 nm MSD in the extreme conditions of smoker versus sCOPD. Similarly, there was a decreasing trend of rapidly moving particle populations with respect to disease severity with the 300 nm MIP. The MSD distribution of 500 nm MIP in sputum was similar regardless of disease severity, with the majority of the particles exhibiting low MSD values, suggesting that 500 nm MIP are significantly larger than the sputum average pore size (Figure 3.3C). Based on these results, subsequent studies were solely assessed against transport of 100 nm MIP.

### *3.3.5 Sputum biochemical composition analysis*

We hypothesized that the biochemical composition might impact the microstructural properties of sputum and, thus, we measured the macromolecular contents of the sputum samples. The percent solids in the sputum collected ranged from

1.1–6.5% by weight, with the higher values primarily associated with more severe disease. The solids content for samples from smokers and COPD patients was 2.4 ± 1.0% and 3.2 ± 1.2% on average, respectively, which is in agreement with previously published values [35]. Sputum from sCOPD patients exhibited the highest percent solids content (3.5 ± 0.7%), while the percent solids for smoker and mCOPD samples were 2.4 ± 1.0% and 3.1 ± 1.4%, respectively (Figure 3.4A). The solids content in the sCOPD group was significantly higher than that in the smoker group ($p < 0.05$). We then compared the percent solids content values with the corresponding 100 nm MIP median $\log_{10}[MSD_{1s}]$, and found that the median $\log_{10}[MSD_{1s}]$ inversely correlated with percent solids (Figure 3.5A; $r = -0.62$, $p<0.0001$).

We next measured concentrations of the primary macromolecules found in sputum, specifically mucin and DNA, and investigated whether there is a relationship between their concentrations and the diffusion rates of 100 nm MIP. The mucin concentration was about 2-fold higher in the amassed COPD sputum samples compared to that from smokers (5.34 ± 3.6 and 2.8 ± 1.1 mg/ml, respectively). Specifically, the severe COPD cohort possessed the highest sputum mucin concentration at 7.9 ± 4.9 mg/ml and was statistically significant compared with that of both the smokers and the mild COPD group (4.1 ± 1.8 mg/ml), respectively (Figure 3.4B, $p<0.01$). The DNA concentration was higher in COPD sputum compared to smoker sputum, averaging 0.24 ± 0.38 and 0.08 ± 0.06 mg/ml, respectively (Figure 3.4C), but it was not statistically significant in this small cohort of patients. When related to nanoparticle diffusion, mucin concentration inversely correlated with the median $\log_{10}[MSD_{1s}]$ of 100 nm MIP (Figure

3.5B; r = -0.62, p=0.0009); however, the relationship was not statistically significant for DNA content and median $\log_{10}[MSD_{1s}]$ of 100 nm MIP (Figure 3.5C; r = -0.22, p=0.23).

### *3.3.6 Relationship between lung function and microstructure*

We hypothesized that the altered sputum microstructure in COPD may correlate with impaired lung function. The median $\log_{10}[MSD_{1s}]$ of 100 nm MIP was positively correlated with the spirometric measurements of $FEV_1/FVC$ (Figure 3.6A; r = 0.39, p=0.03) and $FEV_1$% predicted (Figure 3.6B; r = 0.45, p=0.02). We also compared the spiromic measurements to the solids content which has been shown to be a possible biomarker for lung function [35]. Neither the $FEV_1/FVC$ nor the $FEV_1$% predicted significantly correlated with the sputum percent solids (Figure 3.6C).

### *3.3.7 Statistics*

Statistical significance was determined via a two-tailed Student's t test, assuming unequal variances. Comparisons between multiple groups were determined using one-way analysis of variance (ANOVA) followed by a Tukey post hoc test. Pearson correlation analysis was used to determine r values. Calculations were performed using GraphPad Prism software. P values less than 0.05 were considered significant.

### *3.4 Discussion*

In this preliminary study, we examined whether sputum architecture, reflecting gel pore size, associates with COPD severity and sputum composition. To our knowledge, this is the first analysis of sputum microstructure in COPD patients. We specifically investigated the microstructural properties of spontaneously expectorated sputum from smokers with and without airway obstruction using MPT with muco-inert probes. We showed that dense surface coatings with low molecular weight PEG effectively prevented nanoparticle adhesion to sputum constituents for particles smaller than the mesh spacing, similar to our observations with other mucus secretions, including cervicovaginal mucus [62], respiratory mucus [64], chronic rhinosinusitis mucus [65], and CF sputum [63]. We also demonstrated that the diffusion rates of MIP possessing particle diameter less than the average sputum mesh size (100 nm MIP in this case) can be used to distinguish potentially key biophysical properties of sputum collected from patients with varying disease severity. Using our microstructure measurement we found that a tightened microstructure correlated with lung disease severity as indicated by a decrease in in $FEV_1/FVC$ and $FEV_1$. In addition, patient-specific analysis of sputum microstructure may aid in the development of personalized treatments for effective inhaled therapy. Finally, although not determined here, the mesh spacing (a direct measurement of pore size) of the sputum network may impact the migration of microorganisms [125, 126], including bacteria and immune cells. If so, the mesh spacing measurement can potentially serve as a predictive index of COPD-associated exacerbation, a critical risk factor for COPD [127].

Sputum is a gel that is composed of a complex porous network of solid strands of mucins, DNA and other molecules in an aqueous medium. In order to accurately perform microstructural analysis of the sputum mesh via MPT, the nanoparticle probes must be both non-adhesive and smaller than the average pore size in the sputum mesh [112]. Transport rates of MAP are strongly affected by adhesive interactions with the sputum, whereas MIP resist adhesive interactions with sputum constituents. Due to their muco-inert nature, MIP movement is primarily affected by steric obstruction imposed by the sputum mesh, which makes MIP uniquely appropriate for use in examination of sputum architecture, such as mesh spacing. We found that 100 nm MIP traveled with relatively little resistance through the porous sputum gel samples obtained from both smokers and COPD patients. In contrast, 500 nm MIP, despite their muco-inert surfaces, did not diffuse rapidly in sputum because they are too large to fit through the sputum pores. These findings indicate that 100 nm MIP are optimal to probe the sputum microstructure, whereas conventional mucoadhesive particles (MAP) and MIP larger than the average opening size in the sputum mesh are not suitable for this application.

Biophysical properties of COPD sputum have been relatively underexplored compared to biochemical content analysis, including quantification of pro-inflammatory and bacterial cell markers [128, 129]. Previous biophysical analysis of sputum samples collected from patients with obstructive lung diseases primarily focused on measurement and comparison of macro-rheological properties; for example, the degree of purulence, an indication of infection, in CF sputum samples positively correlated with the bulk viscoelasticity [39]. However, these conventional rheological measurements, while beneficial for understanding macroscopic behavior of the biological fluid, do not provide

direct information on sputum microarchitecture [67, 130]. By combining MIP and the MPT technique to probe sputum microstructure, we discovered a significant correlation between diffusion of 100 nm MIP and disease stage, specifically between sputum samples from smokers and sCOPD patients. The reduction in MIP diffusion rates, as quantified by median $\log_{10}[MSD_{1s}]$, as well as the decrease in the fraction of fast-moving MIP in sCOPD sputum, indicates that the sputum mesh, i.e. pore size, is tighter in severe COPD.

Consistent with previous reports [35, 36], we found a modest increase in the percent solids content of sputum samples from COPD patients compared with that of smokers. The elevation was particularly evident in the severe COPD population. We found a significant inverse correlation between percent solids and the MIP median $\log_{10}[MSD_{1s}]$, suggesting that a greater solids concentration, as can occur with sputum dehydration [36] or mucin hypersecretion, contributes to a tighter sputum mesh in severe COPD. This is in agreement with a previous finding where *in vitro* particle diffusion rates in mucus inversely correlated with solids content [35]. However, it should be noted that this study was conducted with large (1 μm), non-PEGylated (muco-adhesive) particles and, thus, the diffusion readout is more relevant to bulk rheological mucus properties than to microstructural properties such as pore size [131].

Many believe that airway inflammation in obstructive lung disease is linked to perturbation of mucin [132] and/or DNA content [133], which results in elevation of mucus elasticity [106, 134]. We found that the mucin concentration was significantly increased in  in sputum samples collected from COPD patients compared with those from smokers. This is in agreement with a recently published paper from the

SPIROMICS study that found that the total mucin concentration was significantly higher in induced sputum from patients diagnosed with CB compared to those without CB [37]. Further, the mucin concentration corresponded with a tighter sputum microstructure. Additionally the pore size of the mucus mesh can also be affected by the crosslinking density of mucin fibers [134, 135]. Yuan and coworkers have recently reported that oxidation arising from airway inflammation increases the amount of disulfide crosslinks of mucin polymers and, thus, increases the stiffness/elasticity of CF sputum [134]. Increased oxidative stress is also a hallmark of COPD-associated lung disease [136, 137].

We found that sputum microstructural properties correlated with lung function measures (i.e. $FEV_1$/FVC and $FEV_1$ % predicted). In CF sputum, altered sputum rheological properties correlate with bacterial colonization and reduced lung function [138]. The tighter mesh in COPD sputum may also provide a permissive environment for chronic infection and inflammation, perhaps due to reduced bacteria and neutrophil migration coupled with reduced MCC [125]. Thus, microstructure readouts based on MIP diffusion in sputum may find use in the study of disease progression and/or clinical exacerbations. Importantly, there is not a significant relationship between lung function and percent solids thus limiting the solids content as a biomarker for lung disease severity. In particular, MPT analysis with 100 nm MIP appears appropriate for prospective clinical trials and epidemiology studies focused on the modification of sputum properties. Biophysical analysis of COPD sputum by MPT with 100 nm MIP may potentially be used in the future to tailor therapy and to evaluate effectiveness of therapeutics, including mucolytic agents [139]. Finally, our findings invite further analysis of the molecular interactions that contribute to pore size such as disulfide cross-

linking, oxidative modifications and mucin-macromolecule interactions. The approximation of pore size also provides critical measurements for *in vitro* modeling of the mucus gel structure in various disease states.

Of note, the microstructure measurement can only be performed on fresh, spontaneously expectorated sputum in order to preserve the physiological structure and to prevent deterioration observed with prolonged storage or freezing [66]. Induced sputum samples were not used as dilution by inhaled saline during the collection process may alter the physiological microstructure. Thus, the COPD patient population sampled with this method is constrained by the ability to generate a spontaneous specimen.

### *3.5 Conclusion*

Overall, our findings suggest that the characterization of sputum microstructure, available with spontaneous but not induced sputum samples, may provide novel insights into the specific properties of mucus that contribute to COPD pathogenesis. Future studies will focus on the examination of sputum architecture in larger longitudinal cohorts with detailed clinical, physiologic and functional readouts. Such studies could support the use of sputum mesh size as a predictive and personalized index of disease progression.

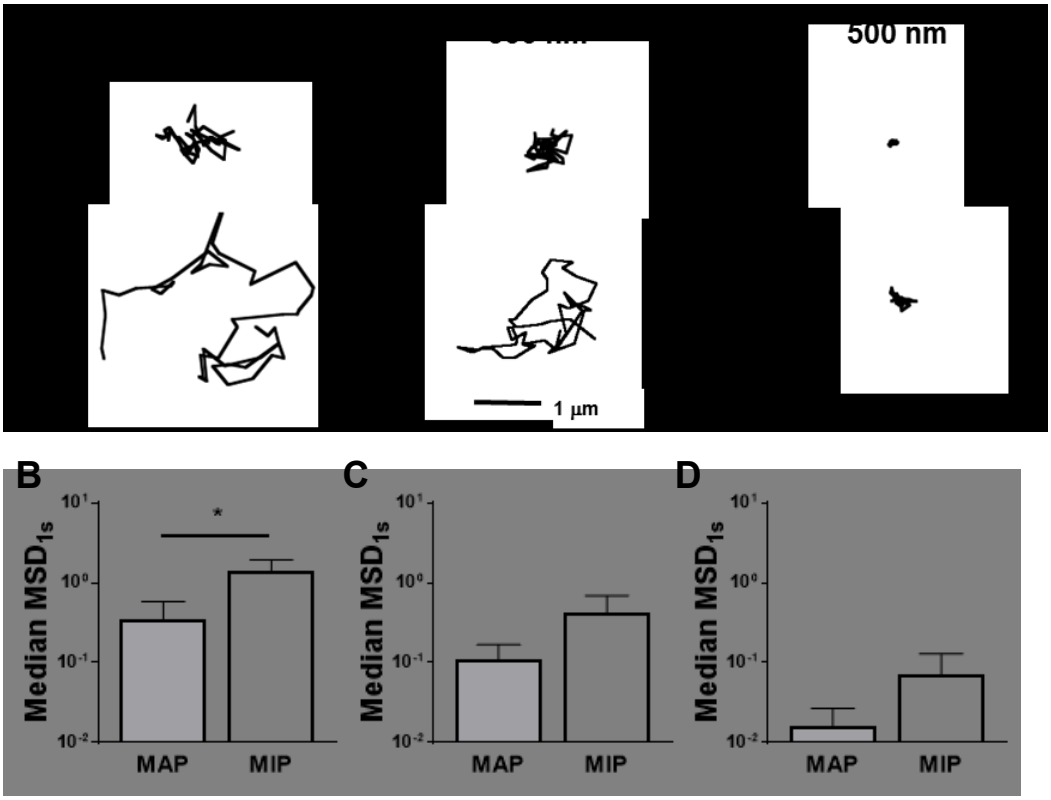


**Figure 3.1. Transport of muco-adhesive and muco-inert polystyrene nanoparticles in spontaneously expectorated sputum from cigarette smokers without airway obstruction.** (A) Representative trajectories of polystyrene nanoparticles possessing nominal sizes of 100, 300, and 500 with (MPP) or without (MAP) the muco-inert PEG surface coating. Trajectories show 3 s of motion. (B-D) Median mean squared displacement (MSD) at a time scale of 1 s for particles with nominal sizes of (B) 100 nm, (C) 300 nm, and (D) 500 nm MAP and MIP. Data represents n=5 sputum samples with at least 500 particles tracked per sample. Error bars represent standard error of the mean. *Denotes statistically significant differences ($p < 0.05$)

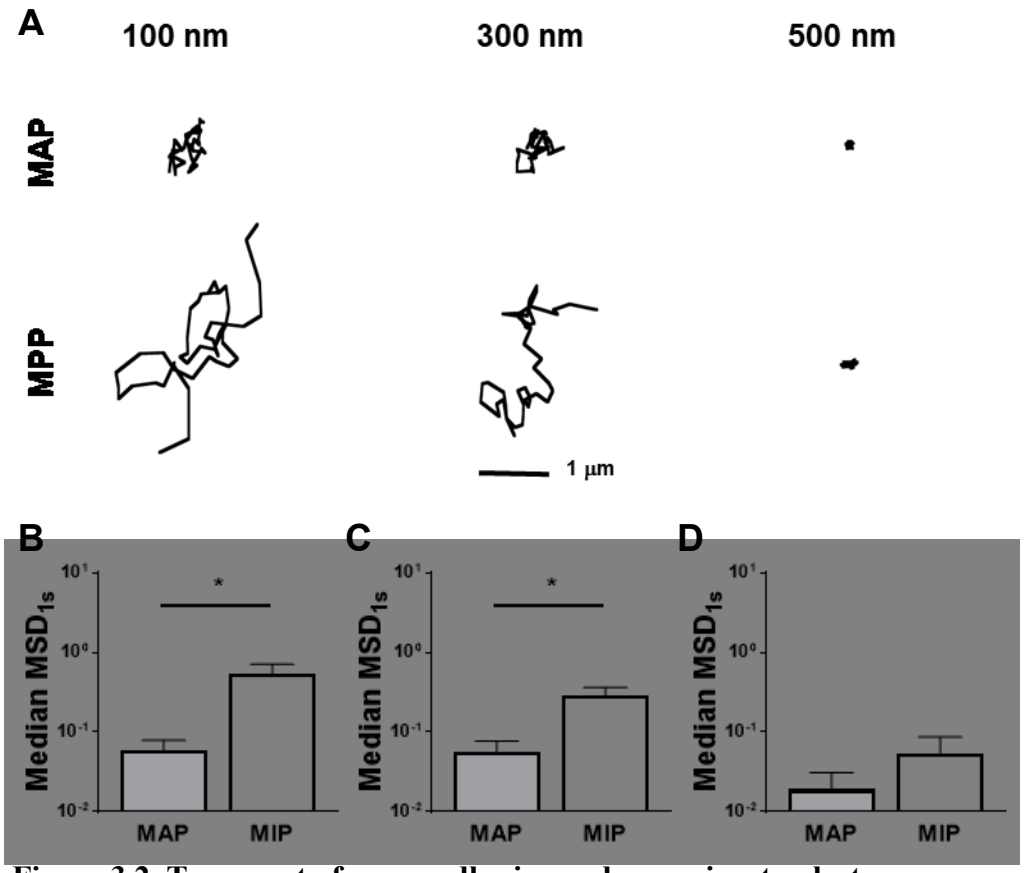


**Figure 3.2. Transport of muco-adhesive and muco-inert polystyrene nanoparticles in spontaneously expectorated sputum from COPD patients.** (A) Representative trajectories of polystyrene nanoparticles possessing nominal sizes of 100, 300, and 500 nm with (MIP) or without (MAP) the muco-inert PEG surface. Trajectories show 3 s of motion. (B-D) Median mean squared displacement (MSD) at a time scale of 1 s for particles with nominal sizes of (B) 100 nm, (C) 300 nm, and (D) 500 nm MAP and MIP. Data represents n=13 sputum samples with at least 500 particles tracked per sample. Error bars represent standard error of the mean. *Denotes statistically significant differences ($p < 0.05$)

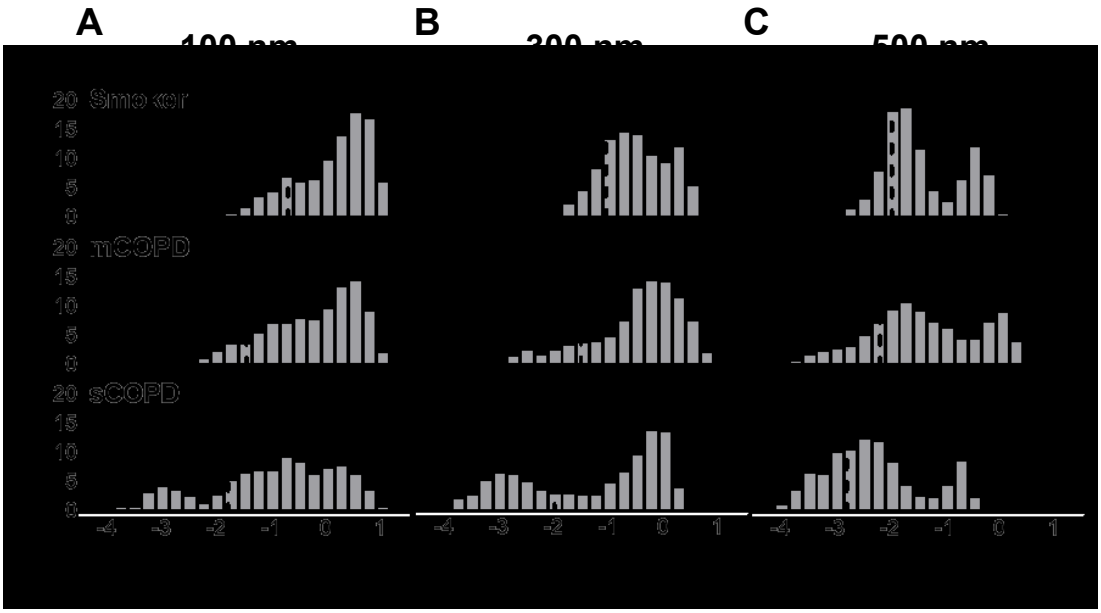


**Figure 3.3. Diffusion of different sized muco-inert nanoparticles in spontaneously expectorated sputum from patients stratified for COPD severity based on spirometric pulmonary function measurements:** cigarette smokers without airway obstruction (Smoker, n=5), mild COPD (mCOPD, n=7), severe COPD (sCOPD, n=6). Distribution of the $\log_{10}[MSD_{1s}]$ of individual MIP with nominal sizes of: (A) 100 nm, (B) 300 nm, and (C) 500 nm. Data represents at least 500 particles tracked per sample. The average median $\log_{10}[MSD_{1s}]$ for each set is indicated by the dashed line.

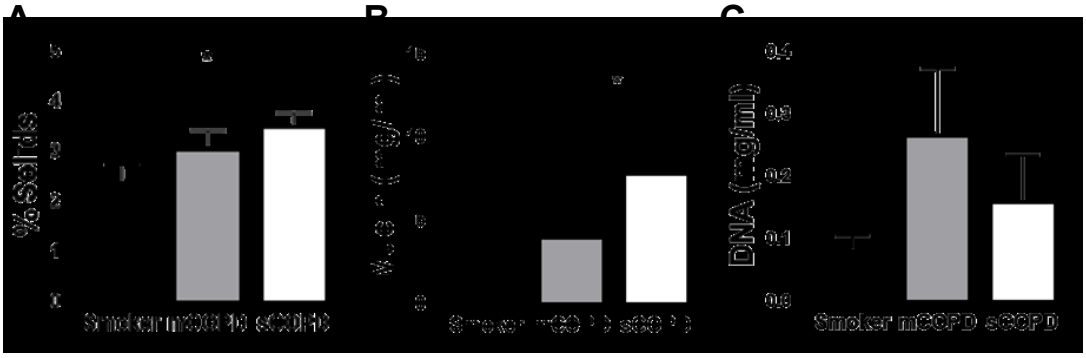


**Figure 3.4. Sputum biochemical contents.** Quantification of (A) percent solids (B) mucin concentration and (C) DNA concentration in sputum from smokers without airway obstruction (Smoker), mild COPD (mCOPD) and severe COPD (sCOPD). Error bars represent the standard error of the mean for each data set. *Denotes statistically significant differences ($p < 0.05$)

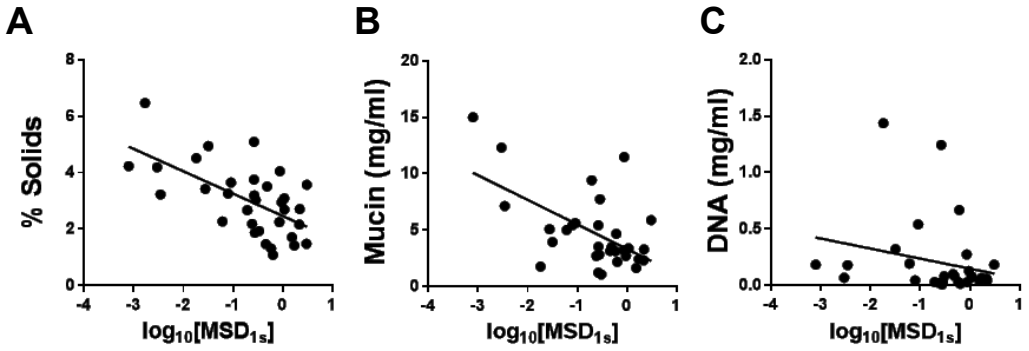


**Figure 3.5. Relationship between sputum microstructure and biochemical components.** Transport of 100 nm MIP (median $\log_{10}[MSD_{1s}]$) inversely correlates with (A) percent solids content ($r = -0.61$, $p < 0.001$) and (B) mucin concentration ($r = -0.57$, $p < 0.001$). (C) The median $\log_{10}[MSD_{1s}]$ does not correlate with DNA concentration ($r = -0.23$, $p = 0.2$).

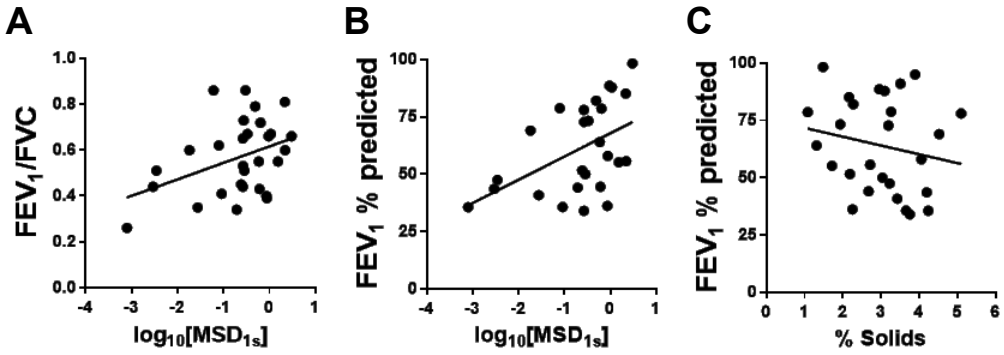


**Figure 3.6. Relationship between sputum microstructure and spirometric measurements.** Transport of 100 nm MIP (median $\log_{10}[MSD_{1s}]$) positively correlates with (A) the ratio of post-bronchodilator $FEV_1$ to FVC ratio ($r = 0.39$, $p < 0.05$) and (B) post-bronchodilator $FEV_1$ % predicted ($r = 0.48$, $p < 0.05$). (C) The percent solids and $FEV_1$ % predicted are not correlated ($r = -0.19$, $p = 0.34$). Spirometry was performed on patients prior to sputum collection.

**Table 3.1.** Participant demographics

| | Smoker<br><br>$FEV_1/FVC>0.7$<br>FVC>LLN | Mild-moderate COPD<br><br>$FEV_1/FVC<0.7$<br>FEV1>50% pred | Moderate-severe COPD<br><br>$FEV_1/FVC<0.7$<br>FEV1<50% pred |
|---|---|---|---|
| N | 9 | 19 | 8 |
| Age | 56.4 (6.78) | 64.8 (9.87) | 71.6 (7.96) |
| | | | |
| Post-BD FEV1 % predicted | 86.30 (17.9) | 63.71 (13.9) | 41.01 (7.9) |
| FEV1/FVC | 0.74 (0.07) | 0.56 (0.08) | 0.38 (0.06) |
| | | | |
| Female, n (%) | 5 (56%) | 9 (47%) | 3 (38%) |
| Current smoker, n (%) | 5 (56%) | 11 (58%) | 4 (50%) |

nit of normal.

bronchodilator

ed as mean (SD) unless otherwise indicated.

**Table 3.2.** Participant demographics for microstructural analysis

| | Smoker<br><br>$FEV_1/FVC>0.7$<br>FVC>LLN | Mild-moderate COPD<br><br>$FEV_1/FVC<0.7$<br>FEV1>50% pred | Moderate-severe COPD<br><br>$FEV_1/FVC<0.7$<br>FEV1<50% pred |
|---|---|---|---|
| N | 5 | 7 | 6 |
| Age | 53.4 (7.09) | 59.17 (6.46) | 66.17 (11.65) |
| Pack-years | 46.7 (17.59) | 55.38 (19.18) | 60.58 (21.90) |
| | | | |
| Total exacerbations | 1 (1.22) | 0.67 (0.82) | 0.5 (0.84) |
| Post-BD FEV1 % predicted | 87.18 (8.47) | 59.03 (8.96) | 38.32 (3.41) |
| Post-BD FVC % predicted | 96.1 (12.82) | 80.75 (6.36) | 81.3 (17.80) |
| FEV1/FVC | 0.73 (0.06) | 0.59 (0.07) | 0.38 (0.06) |
| | | | |
| African American, n (%) | 3 (60%) | 2 (29%) | 1 (17%) |
| Female, n (%) | 3 (60%) | 3 (43%) | 1 (17%) |
| Current smoker, n (%) | 4 (80%) | 5 (71%) | 5 (83%) |
| Usual cough, n (%) | 4 (80%) | 3 (43%) | 5 (83%) |
| Usual phlegm, n (%) | 3 (60%) | 3 (43%) | 4 (67%) |

e indicated.

**Table 3.3.** Nanoparticle physicochemical characterization

| Nominal Size (nm) | Functionalization | Diameter[a] (nm) | PDI[a] | ζ-potential[b] (mV) |
|---|---|---|---|---|
| 100 | PSCOOH | 88 ± 1 | 0.02 | -52 ± 1 |
| 100 | PSPEG | 109 ± 2 | 0.02 | -7 ± 1 |
| 300 | PSCOOH | 292 ± 4 | 0.01 | -75 ± 6 |
| 300 | PSPEG | 318 ± 7 | 0.04 | -4 ±1 |
| 500 | PSCOOH | 538 ± 11 | 0.05 | -52 ± 1 |
| 500 | PSPEG | 553 ± 5 | 0.05 | -4 ± 1 |

[a] Hydrodynamic diameter and PDI measured by dynamic light scattering.

[b] Measured in 10 mM NaCl at pH 7.4.

# 4. Formulation of telmisartan nanoparticles for the local treatment of COPD

## *4.1 Introduction*

Transforming growth factor (TGF)-β is a multifunctional regulator of cell growth and differentiation during organ development and plays a critical role in lung development and repair [80, 81]. TGF-β and the signaling is tightly controlled to maintain physiological homeostasis in the healthy lung [82]. Alterations in TGF- β expression is associated with COPD development and progression, and elevated TGF- β levels have been shown in both the airway and airspace compartments of patients with COPD. Further, in pre-clinical models, cigarette smoke exposure increases TGF-β signaling throughout the lung parenchyma, thereby triggering oxidative stress injury, inflammation, epithelial cell death and airway remodeling [84-88]. These processes likely culminate in the small airway obstruction and airspace destruction that are hallmarks of COPD. Thus, TGF- β signaling is an especially attractive candidate pathway that can be targeted for COPD treatment.

Therapeutic interventions that antagonize TGF-β signaling may halt progression and/or reverse the pathogenesis of COPD. Angiotensin receptor blockers (ARB), specific antagonists of the angiotensin II type 1 receptor (AT1R), are antihypertensive agents widely utilized in the clinic. AT1R is expressed on the surface of airway and alveolar epithelial cells as well as lung vasculature [140, 141]. Importantly, ARB suppress *de novo* TGF-β expression [142-144] as well as extracellular activation of latent TGF-β [142-146] via AT1R antagonism. Previously, we demonstrated that daily oral

administration of an ARB, losartan (LOS), inhibited TGF- β signaling, and effectively protected against damage in the lungs of a chronic CS-exposed mouse model of COPD [85]. However, the high drug dose and frequent administration of the drug concentration required for TGF-β antagonism may result in adverse systemic side effects, which is especially important in elderly populations.

Inhalation is a non-invasive route for the delivery of drugs locally to the lungs. Inhaled delivery provides direct, topical delivery of the drug to the site of disease while negating first pass metabolism and reducing systemic exposure of the therapeutic [40-43]. Unfortunately, inhalation of free drugs can be rapidly removed via systemic absorption and mucociliary clearance [45, 46], reducing the time that the drug concentration remains in the therapeutic window. Encapsulation in nanoparticles can address the limitations of conventional pulmonary delivery by improving lung drug levels over time and allow for reduced dose and/or dosing frequency. Thus we sought to engineer a nano-based ARB formulation for pulmonary delivery. In this study we used the ARB telmisartan (TEL) instead of LOS due to its readily active nature unlike LOS that requires hepatic activation [147, 148] and its intrinsically higher affinity to AT1R than LOS [149].

Previously we have established the design criteria for inhaled NP, specifically that the particles must be smaller than the respiratory mucus pore size, densely coated with poly(ethylene glycol) (PEG) to minimize interactions with the mucus, and stable in physiological conditions [70, 78]. We first attempted to encapsulate TEL in NP composed of the biodegradable polymer poly(lactic-co-glycolic acid) (PLGA); however, due to challenges with effectively loading TEL in PLGA we instead engineered a nanocrystal (NC) formulation with TEL (TEL-NC) for the localized treatment of COPD.

## *4.2 Methods*

### *4.2.1 Formulation of biodegradable TEL NP - Emulsion method*

Nanoparticles were prepared by a single emulsion method. Briefly, polymer (40 mg, 75 mg/ml) and TEL (4 mg) were dissolved in dichloromethane (DCM) and sonicated in an aqueous phase of 5 ml of 0.5 % (w/v) emulsifier at 30% amplitude for 2 ml Vibra-Cell$^{TM}$ VCX-500 probe sonicator. The emulsion was then poured into 35 ml of 0.5% emulsifier under magnetic stirring (700 rpm) for 3 hours to evaporate the organic solvent. The nanoparticle suspension was filtered with a 1 um filter to remove aggregates before collection via centrifugation at 10,000*g* for 30 min. Nanoparticles were thoroughly washed and suspended in water. Various polymers and polymer combinations were tested, specifically PLGA$_{45k}$-PEG$_{5k}$ (PLGA-PEG), a blend of PLGA2A and PLGA$_{15k}$-PEG$_{5k}$ (PLGA/PLGA-PEG), PLA$_{45k}$-PEG$_{5k}$, (PLA-PEG) and a blend of PLA and PLA4$_{5k}$-PEG$_{5k}$ (PLA/PLA-PEG). The emulsifiers tested were sodium cholate (CHA) and saponin.

### *4.2.2 Formulation of biodegradable TEL NP - Zinc chelation method*

PLGA15k-PEG5k (15 mg), PLGA1A (10 mg), and TEL (2.5 mg) were dissolved in THF. ZnCl dissolved in THF was added to the polymer drug solution at various concentrations and incubated for 1 hour at room temperature. The THF solution was slowly added dropwise using a syringe into 30 ml of 5% F127 under magnetic stirring (700 rpm) for 2 hours to evaporate organic solvent. Subsequently, 0.5 ml of 0.5 M ethylenediaminetetraacetic acid (EDTA) was added to the nanoparticles to chelate excess zinc and remove free drug. The NP suspension was filtered with a 1 um filter to remove

aggregates before collection via centrifugation at 10,000*g* for 30 min. NP were thoroughly washed and resuspended in water.

### *4.2.3 Characterization of TEL NP*

NP diameter and ζ-potential were measured via dynamic light scattering (DLS) and laser Doppler anemometry, respectively, using a Zetasizer Nano ZS (Malvern Instruments) in 10 mM NaCl at pH 7.4

### *4.2.4 TEL drug loading in biodegradable NP*

To measure the telmisartan content in the nanoparticles, a known amount of NP was frozen in liquid nitrogen, lyophilized, weighed and dissolved in a 50/50 mixture of methanol and 10 mM ammonium acetate. For the zinc chelation NP, 0.2 ml of 0.5 M EDTA was added and incubated for 30 min first. The TEL concentration was measured via reverse-phase high-performance liquid chromatography (HPLC). The mobile phase was composed of methanol and 10 mM ammonium acetate (35:65 v/v) containing 0.1% trifluoroacetic acid at a flow rate of 1 ml/min. Column effluent was monitored by UV detection at 240 nm. The drug loading was calculated based on the following equation:

$$Drug\ loading\ (\%) = \frac{telmisartan\ (\mu g)}{particles\ (\mu g)}$$

### *4.2.5 Formulation of TEL-NC*

TEL and Pluronic F127 or Pluronic F68 (abbreviated as F127 and F68 hereafter, respectively) were dissolved in 2 ml of chloroform at a 1:4 mass ratio. The chloroform was rapidly evaporated with a nitrogen gas stream to create a film. The film was further

dried via vacuum overnight. The film was hydrated with ultrapure water and incubated for 20 minutes at room temperature followed by bath sonication for 10 minutes. The suspension was further homogenized with a Vibra-Cell$^{TM}$ VCX-500 probe sonicator for 30 minutes with a pulse of 1 second on 1 second off at 100% amplitude. The resultant suspension was centrifuged at 2000 rpm for 5 minutes to remove any large particulates. The TEL-NC were collected via centrifugation at 21130x*g* for 10 minutes and were resuspended in ultrapure water. TEL was dissolved in methanol and the drug concentration was measured using a spectrofluorophotometer (Shimadzu) at excitation 300 nm and emission 360 nm with a slit width of 3 for both the excitation and emission. The TEL free drug (TEL-FD) was prepared by crushing Micardis® tablets into a powder and creating a suspension in water or fully dissolving the powder in 10% DMSO-water (v/v).

### *4.2.6 Characterization of TEL-NC*

Transmission electron microscopy (TEM) was performed to visualize the drug formulations. F127/TEL-NC, F68/TEL-NC, or TEL-FD were diluted in water and 10 µl of each formulation was added to copper TEM grids and incubated for 15 minutes. The remaining droplet was removed via wicking with filter paper. The grids were allowed to dry overnight and were subsequently imaged on a Hitachi H7600 microscope at 30k magnification. The dimensions of the F127/TEL-NC and F68/TEL-NC were measured with ImageJ software. F127/TEL-NC, F68/TEL-NC, or TEL-FD) were diluted in ultrapure water and the hydrodynamic diameter was measured via dynamic light

scattering (DLS) with a Zetasizer Nano ZS (Malvern). The zetapotential was measured vial laser Doppler anemometry in 10mM NaCl at pH 7.4 with a Zetasizer NanoZS.

### *4.2.7 Animals*

All animal protocols were approved by the Institutional Animal Care and Use Committee at the Johns Hopkins Medical Institutions. Female CF-1 mice or male Wistar rats (6-8 weeks, Harlan) were allowed to acclimate for 1-2 weeks before handling, with access to food and water ad libitum throughout the experiments.

### *4.2.8 Stability of TEL-NC in bronchial alveolar lavage fluid (BALF)*

Bronchial alveolar lavage fluid (BALF) was collected by sequentially lavaging mouse lungs three times with 1 ml of PBS. The cells were separated by centrifugation and discarded. The supernatant was collected and syringe filtered (0.2 mm). Twenty microliters of F127/TEL-NC or F68/TEL-NC solution was added to 0.8 ml of BALF and incubated at 37ºC. The hydrodynamic diameter was measured by DLS at various time points.

### *4.2.9 Macrophage uptake*

Murine alveolar macrophages (MH-S, ATCC) were cultured. 10 mM of F127/TEL-NC, F68/TEL-NC, or TEL-FD was added to the cells and incubated for 2 hours at 37ºC. Cells were detached using cell scrapers and centrifuged at XX. The supernatant was removed and the cells were resuspended in pH 3 MeOH to extract TEL. The cells were lysed in a bullet blender at XX conditions. The homogenates were

centrifuged at 21130x*g* for 10 minutes and the supernatant was collected. TEL concentration was measured via a spectrofluorphotometer as described above.

### *4.2.10 Measurement of $[Ca^{2+}]_i$ in pulmonary artery smooth muscle cells*

Primary (pulmonary artery smooth muscle cells) PASMCs were isolated from rats as previously described [150]. Briefly the heart and lung were excised and transferred to a petri dish with HEPES-buffered saline solution (HBS). The intrapulmonary arteries were isolated and the tissue was digested for 20 min at 37ºC in reduced $Ca^{2+}$ HBS containing collagenase (type I, 1750 U/ml), papain (9.5 U/ml), bovine serum albumin (2 mg/ml), and dithiothreitol (1 mM). Individual smooth muscle cells were collected and the cell suspension was filtered. Cells were cultured in Ham's F-12 media supplemented with 0.5% fetal calf serum and 1% penicillin-streptomycin for 24–48 h.

$[Ca^{2+}]$ was measured as previously described [151]. Briefly, PASMCs were plated at 50–60% confluence on glass coverslips and loaded with 5 μM Fura 2-AM for 1 h at 37°C before being placed in a temperature-controlled (37°C) laminar flow chamber in a live cell $Ca^{2+}$ imaging system. Cells loaded in the flow chamber were perfused with warmed modified Krebs solution and bubbled with 16% $O_2$ gas at 37°C. The flow chamber and perfusates were maintained at 37°C. At the beginning of each experiment, cells were perfused for 15 min to allow for establishment of stable baseline. $[Ca^{2+}]_i$ was calculated from the $F_{340}/F_{380}$ of $Ca^{2+}$ calibration solutions. Cells were pretreated with PBS only or 50 μM of TEL as F127/TEL-NC or TEL-FD for 30 min prior to ANGII (1 μM) exposure.

### *4.2.11 Measurement of fibronectin content*

Primary pulmonary fibroblasts were isolated and cultured as previously described [152]. The lungs were harvested, minced with a razor blade and incubated in DMEM F-12 media (Gibco) containing collagenase (type I, 2 mg/ml) at 37ºC for 30 minutes. The resulting cell suspension was washed with DMEM F-12 media supplemented with 15% FBS and 1x penicillin/streptomycin, centrifuged to collect cells and transferred to a culture flask. For the fibronectin measurement, the cells were incubated with 5 ng of TGF-β for 1 hour before TEL treatment. 25 μm of F127/TEL-NC or TEL-FD was added to the cells and exposure lasted 24 hours. Fibronectin content was measured via Western blot. Membranes were incubated with the primary antibody for 1 hour at room temperature. Detection was by the Pierce West Dura system (Pierce Biotechnology, Rockford, IL).

### *4.2.12 Statistics*

Statistical significance between treatment groups was determined via a two-tailed Student's t test, assuming unequal variances. Comparisons between multiple groups were determined using one-way analysis of variance (ANOVA) with Tukey's post hoc test. Calculations were performed using GraphPad Prism software. P values less than 0.05 were considered significant.

## *4.3 Results*

### *4.3.1 Preparation and characterization of polymer-based NP*

We first attempted to encapsulate TEL in PLGA-PEG via a single emulsion method using the small molecule CHA as an emulsifier. We have previous used CHA to load various hydrophobic drugs in PLGA NP [115, 153]. While this method produced small NP (133 nm) with a low PDI of 0.06 and near neutral charge (-6 mV), the drug loading was very poor, less than 1% (Table 4.1). We also tested various polymer and drug concentrations, but neither of these parameters had an effect on the TEL loading. We next tried an alternative small molecule emulsifier, saponin, that we have previously used [153]. Unlike the anionic CHA, saponin is neutrally charged. Once again, the physicochemical characteristics of the PLGA-PEG NP produced with saponin were positive with an average size of 178 nm, PDI of 0.1 and ζ-potential of -5.3 mV; however, while saponin improved the drug loading compared with CHA, the average drug loading achieved was only 2.3% (Table 4.1). We next altered the polymer composition in an attempt to increase the drug loading. We tested a blend of unPEGylated and PEGylated PLGA (PLGA/PLGA-PEG), PLA-PEG, and a blend of unPEGylated and PEGylated PLA (PLA/PLA-PEG). The blending approach for both PLA and PLGA resulted in the highest drug loadings; however, we were still unable to achieve TEL drug loading > 4% (Table 4.2).

As an alternative to the conventional emulsion method, we also investigated whether bridging the TEL and polymer via chelation with zinc would improve the drug loading in PLGA-PEG NP. It has previously been shown that addition of zinc improves the loading of phosphate drugs in PLGA NP likely by forming an ionic bridge between

the terminal carboxyl groups on the polymer and the phosphate groups on the drugs [154-156]. TEL also has a carboxyl group, thus we hypothesized that the zinc may interact with the carboxyl groups on both the drug and polymer. For this method we formulated the NP via a solvent diffusion method as opposed to an emulsion method. The physicochemical characteristics are displayed in Table 4.3. This method produced small NP with diameter around 110 nm with PDI < 0.1 and a near neutral ζ-potential; however, the zinc chelation provided little improvement to the drug loading (~1%). Further, increasing the ZnCl concentration had no effect on the drug loading (Figure 4.1).

### *4.3.2 TEL-NC formulation and physicochemical properties*

Due to the inability to achieve sufficient drug loading of TEL in polymeric-based NP, we instead pursued an alternative approach drug nanocrystals. Adapting a method previously used to produce curcumin NC [78], we formulated telmisartan nanocrystals (TEL-NC) using a combined bottom up and top down approach by first creating a film with the drug and stabilizer followed by hydration and high powered probe sonication. We developed two TEL-NC formulations with Pluronic F127 (F127/TEL-NC) or Pluronic F68 (F68/TEL-NC) as the stabilizer.

The average hydrodynamic diameters measured by dynamic light scattering (DLS) were ~100 nm for F127/TEL-NC and ~250 nm for F68/TEL-NC (Table 4.4). TEM revealed that both NC formulations were rod-shaped, but the (F68/TEL-NC were larger in size than the F127/TEL-NC (Figure 4.2A and 4.2B), in agreement with the DLS results. Size measurements of an aqueous suspension of free drug (TEL-FD) by both DLS and TEM revealed larger than micron size aggregates (Table 4.4 and Figure 4.2C). These

findings suggest that F127 stabilized the surface of NC during formulation better than F68. To confirm the colloidal stability in a physiologically relevant environment, we measured hydrodynamic diameter over time via DLS of the F127/TEL-NC and F68/TEL-NC formulations in murine BALF at 37ºC. The hydrodynamic diameter of the F127/TEL-NC remained stable for at least 24 h, whereas F68/TEL-NC rapidly aggregated (> 1000 nm) in the same conditions (Figure 4.2D). Further, the F127/TEL-NC remained stable in aqueous conditions for at least 25 days as indicated by little change in the hydrodynamic diameter and PDI during that period of time (Figure 4.2E).

### *4.3.3 Alveolar macrophage uptake*

Additionally, we investigated the effect on the stabilizer on the ability to avoid clearance by mouse alveolar macrophages. We found that ~10- and 4-fold more drug was uptaken in mouse alveolar macrophages *in vitro* when administered as TEL-FD and F68/TEL-NC compared with F127/TEL-NC, respectively (Figure 4.3). Based on these results all subsequent studies were performed with the optimal F127/TEL-NC formulation.

### *4.3.4 In vitro activity of F127/TEL-NC*

Next we confirmed that the nano-formulation process did not impact the drug's intrinsic properties. We first tested the *in vitro* activity of F127/TEL-NC in primary pulmonary artery smooth muscle cells (PASMC) isolated from rats. Angiotensin II (ANG II) binding to the AT1R causes vasoconstriction and a transient elevation of intracellular calcium ($iCa^{2+}$) levels, which is inhibited by ARB [157, 158]. Thus, drug activity can be

determined by measuring $iCa^{2+}$ concentration in response to ANG II exposure following a pretreatment of ARB. Cells exposed to vehicle solutions, including F127 or PBS alone, exhibited a sharp increase of $iCa^{2+}$ levels in response to ANG II (Figure 4.4A). In contrast, TEL either dosed as F127/TEL-NC or free drug, effectively blocked the elevation of $iCa^{2+}$ (Figures 4.4B and 4.4C), suggesting that the drug activity was retained after NC formulation.

### *4.3.5 Antagonism of TGF-β expression by F127/TEL-NC*

TGF-β is a pro-fibrotic protein that induces expression of matrix protein fibronectin in fibroblasts [159, 160], a hallmark of pathogenesis in lung injury [161, 162]. We thus investigated the effect of F127/TEL-NC on the TGF-β-dependent fibronectin expression in isolated primary mouse lung fibroblasts. As shown in Figure 4.5, we found that both TEL-FD and F127/TEL-NC reversed fibronectin expression induced by TGF-β signaling (right, $p<0.05$). Of note, the media control exhibited some level of fibronectin expression mediated by supplemental TGF-β required for maintaining fibroblast cell viability *in vitro*, which was reversed by both TEL-FD and F127/TEL-NC (left, $p<0.05$), similar to the case of additional TGF-β treatment.

### *4.4 Discussion*

Here we engineered a nanocrystal formulation of TEL suitable for pulmonary delivery (F127/TEL-NC). We demonstrated that the optimized NC formulation remained stable in a physiologically relevant environment, evaded clearance via alveolar macrophages and maintained the intrinsic drug properties. We first attempted to encapsulate TEL in PLGA NP; however, despite testing multiple parameters and methods we were unable to achieve significant drug loading. Fortunately the very poor water solubility of TEL allowed us to purse an alternative approach. Further, the F127/TEL-NC formulation has significant advantages over polymer-based NP for pulmonary administration. The F127/TEL-NC are solely composed of generally regarded as safe (GRAS) materials, specifically pure drug and allow for high drug loading with limited excipients since the particles are composed solely of drug and Pluronic. The F127/TEL-NC formulation has significant advantages compared to free drug and drug formulated in polymer-based nanoparticles for pulmonary administration. The F127/TEL-NC are composed solely of TEL and Pluronic F127 both of which are FDA approved products. F127 is a Generally Regarded as Safe (GRAS) material and is widely found in in pharmaceutical products [79, 163]. Further, since the formulation is solely composed of drug and F127 concern over accumulation and potential toxicity of carrier polymers with repeated administrations is eliminated.

Importantly, the nanonization process did not affect the intrinsic activity of the drug. Nanonization especially of hydrophobic drugs has become widely used in industry. In general, this process increases the particulate surface area to volume ratio which results in improved solubility and thus bioavailability of the drug. There are many drug

nanocrystals currently manufactured and used in the clinic or being tested in clinical trials preclinical development [73, 76, 77]. Thus, feasibility for scale up and reproducible manufacture of new NC are promising. Further, nanosuspensions can be readily nebulized as an aerosol for pulmonary delivery [73]. A nanosuspension composed of the corticosteroid budesonide was able to be nebulized and the size distribution was not affected by nebulization [164, 165]. More recently, a nebulized budesonide nanosuspension formulation was well tolerated in healthy adults in initial clinical trials and was nebulized faster compared to the commercially available formulation [166]. In a preclinical study in mice, nebulization of a nanosuspension formulation with the corticosteroid fluticasone exhibited dose proportional concentrations in the lungs and decreased systemic exposure [167]. The simplicity of the composition and the well-established industrial practice result in lower regulatory barriers for the development of new NC products.

The ability of F127/TEL-NC to retain colloidal stability in physiological fluid in the lung is of great importance, since aggregated NC can be cleared either via mucocililary clearance in the airways or alveolar macrophages in the airspace [17, 45, 46]. We have previously determined the design criteria required for nanoparticles to evade both mucociliary and alveolar clearance and thus be retained longer in the lungs [70, 168]. We found that coating hydrophobic PLGA nanoparticles with Pluronic F127 delayed clearance from mouse lungs thus increasing the drug residence time in the lungs. We have applied this same strategy to formulate NC for inhaled delivery. The F127/TEL-NC formulation was adapted from a method to engineer NC that are capable of penetrating lung mucus [78]. Model curcumin NC produced with F127 but not those with

F68 were capable of diffusing in sputum from cystic fibrosis patients and also uniformly distributed along the mucus coated airways in mice. Unfortunately, we were unable to evaluate the mucus penetrating capability of our F127/TEL-NC formulation. While TEL possesses intrinsic fluorescence, the spectrum (300/360 nm) is in the ultraviolet region [169] and overlaps with the mucus autofluorescence. Further, conjugation of a fluorophore to the drug could potentially alter the drug properties (i.e. hydrophobicity) and would significantly increase the molecular weight of the compound both of which could impact the nanocrystal formulation. However, the same properties that make nanoparticles muco-inert (i.e. dense surface PEGylation) also prevent uptake and thus clearance via alveolar macrophages [170, 171]. In agreement with previous studies [172, 173], we showed that the F127 coating minimized drug uptake by mouse alveolar macrophages compared with F68 and a free drug suspension.

The difficulties in effectively encapsulating TEL in PLGA NP were unexpected. We have previously formulated biodegradable polymer-based particles with various hydrophobic drugs including paclitaxel [115, 174], curcumin [153], BPTES [175], and etoposide [176]. Further, we have successfully employed zinc chelation to load drugs in PLGA NP [70, 156]. However, in this case the zinc was used to transform water soluble drug with a phosphate group into a hydrophobic complex and thus resulted in improved drug loading [70, 154-156]. TEL is highly lipophilic and while it is extremely insoluble in water, the solubility of TEL is pH dependent and it is soluble in most strong acids and bases [177]. Due to the presence of a carboxyl group TEL is a weak acid with a pKa of 4.45. Thus it is possible that TEL and PLGA (or PLA) which also possess carboxyl groups are incompatible.

## *4.5 Conclusion*

We engineered a nanocrystal formulation of the angiotensin receptor blocker, telmisartan, for the local treatment of COPD composed solely of drug and a GRAS stabilizer. The F127/TEL-NC were stable both in physiologically relevant conditions and in a water suspension at room temperature. Further, the F127 coating inhibited macrophage uptake. Importantly the formulation process did not affect the intrinsic drug properties and the F127/TEL-NC were capable of reducing TGF-β expression *in vitro*.

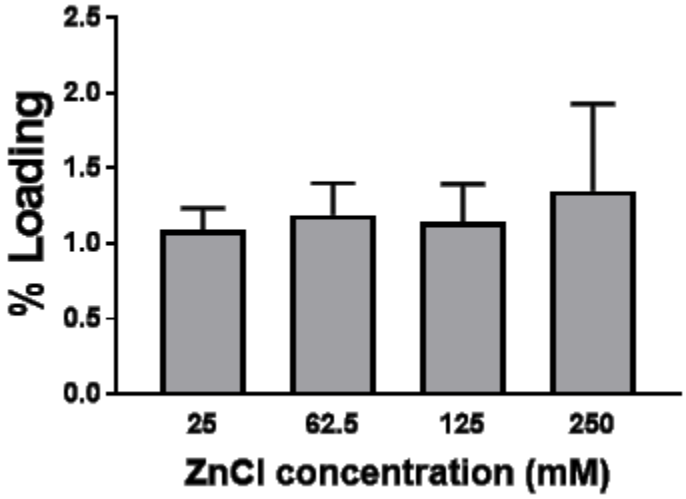


**Figure 4.1. The effect of zinc chloride concentration on telmisartan drug loading in PLGA-PEG nanoparticles.**

Error bars represent standard error of the mean.

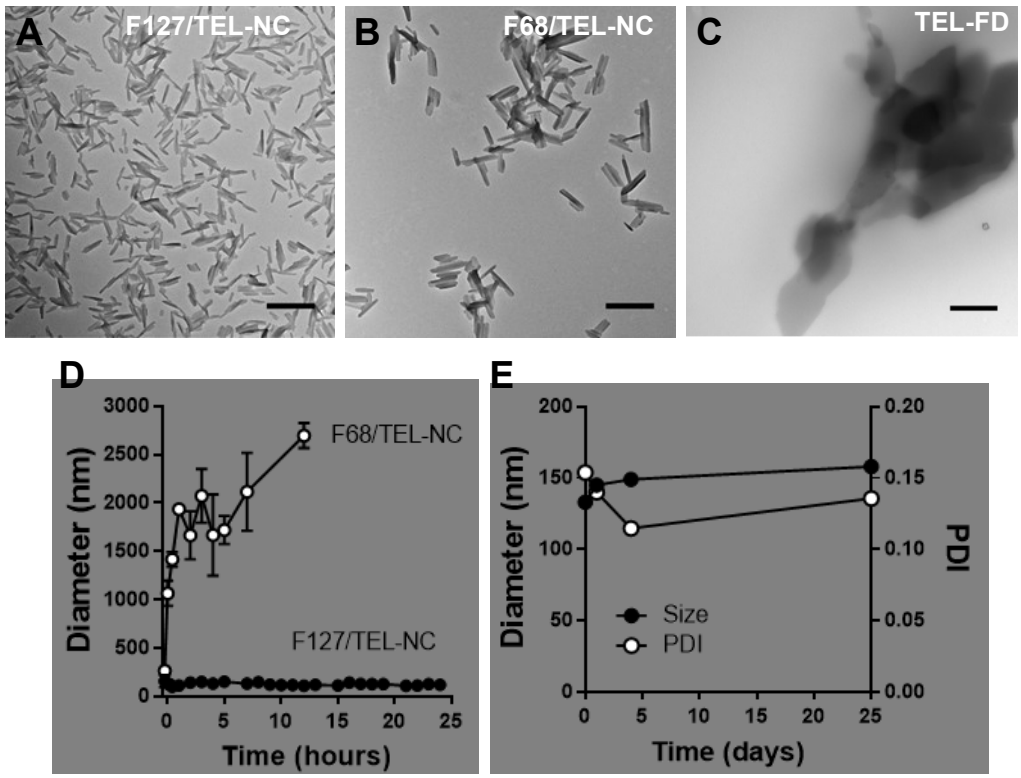


**Figure 4.2 TEL-NC formulation and characterization.** Representative TEM images of (A) F127/TEL-NC, (B) F68/TEL-NC and (C) free drug (TEL-FD) (scale bar = 500 nm). (D) Colloidal stability of F127/TEL-NC and F68/TEL-NC in murine bronchial alveolar lavage fluid (BALF) at 37°C. (E) Colloidal stability of F127/TEL-NC suspension in water at room temperature over time. Error bars represent standard error of the mean.*Denotes statistically significant differences ($p < 0.05$)

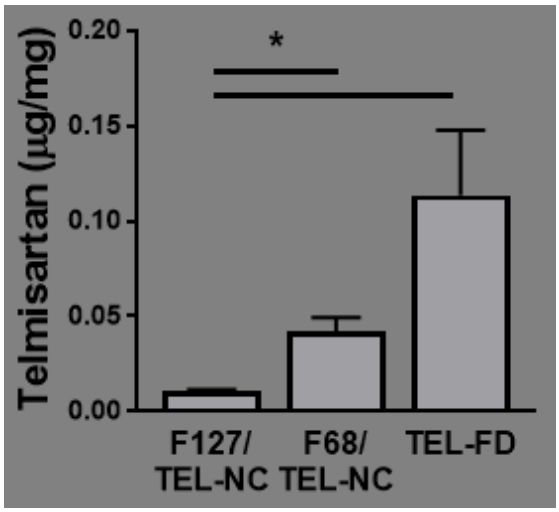


**Figure 4.3. Uptake of telmisartan formulations in mouse alveolar macrophages.** MH-S cells were incubated with 10 mM of F127/TEL-NC, F68/TEL-NC or TEL-FD for 2 hours. Drug concentration was measured in cell lysates. Error bars represent standard error of the mean. *Denotes statistically significant differences ($p < 0.05$)

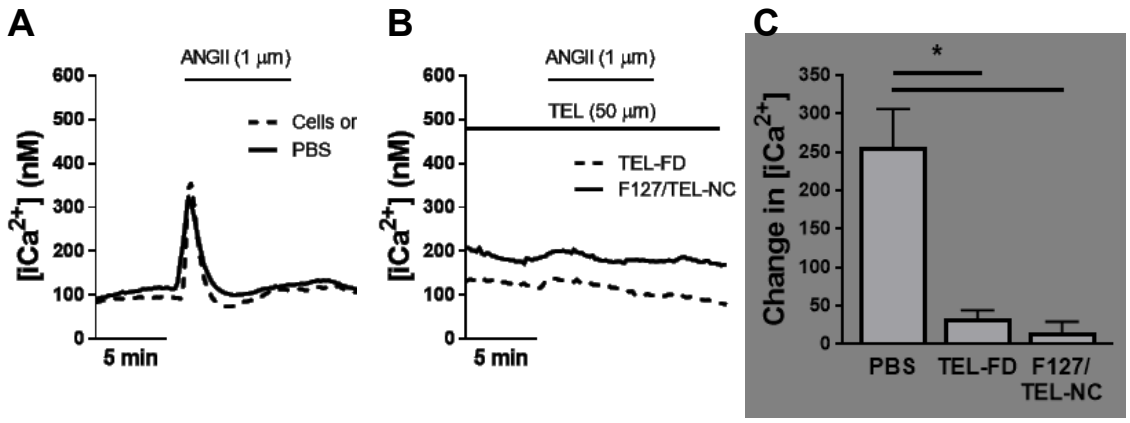


**Figure 4.4. F127/TEL-NC antagonizes ANGII binding to ATR1.** PASMC were pretreated with PBS or different dosing formulations of TEL for 30 min prior to exposure to ANG II. Representative traces of mean $iCa^{2+}$ concentration in response to ANG II (n = 25 cells each) for (A) vehicle controls and (B) TEL-FD and F127/TEL-NC. (C) Quantified change in $iCa^{2+}$ concentration after the pretreatment with TEL-FD and F127/TEL-NC. Error bars represent standard error of the mean.*Denotes statistically significant differences ($p < 0.01$)

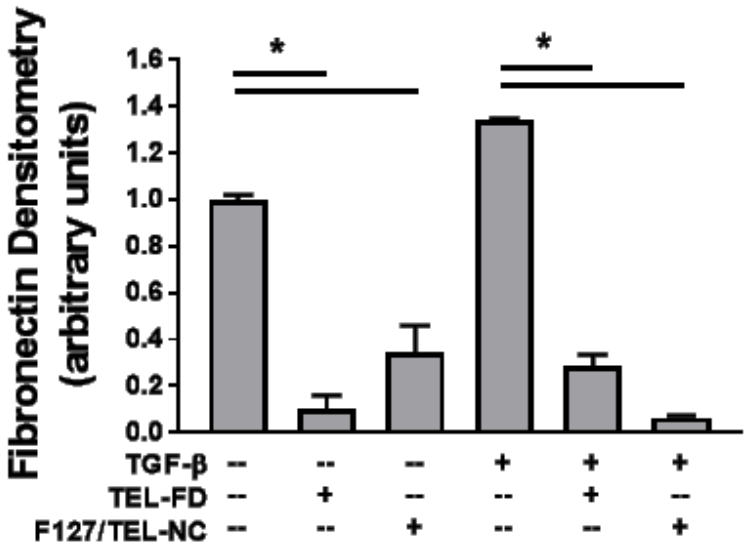


**Figure 4.5. Inhibition of TGF-β-dependent fibronectin expression in mouse primary lung fibroblasts.** Effect of TEL-FD and F127/TEL-NC (at 25 mM TEL concentration) on TGF-β expression in media alone (left) and in the presence of exogenous TGF-β (right). Error bars represent the standard error of the mean. *Denotes statistically significant differences ($p < 0.01$)

**Table 4.1** Charaterization of biodegradable telmisartan nanoparticles produced by the emulsion method: effect of emulsifier

| Polymer | Emulsifier | Diameter[a] (nm) | PDI[a] | ζ-potential[b] (mV) | Drug loading (%) |
|---|---|---|---|---|---|
| PLGA-PEG5k | 0.5% CHA | 133 ± 6 | 0.06 | -6.0 ± 1.7 | 0.4 |
| PLGA-PEG5k | 0.5% saponin | 178 ± 22 | 0.10 | -5.3 ± 1.6 | 2.3 |

[a] Hydrodynamic diameter and polydispersity index (PDI) measured by dynamic light scattering.

[b] Measured in 10 mM NaCl at pH 7.4.

**Table 4.2** Charaterization of biodegradable telmisartan nanoparticles produced by the emulsion method: effect of polymer

| Polymer | % PEG | Diameter[a] (nm) | PDI[a] | ζ-potential[b] (mV) | Drug loading (%) |
|---|---|---|---|---|---|
| PLGA-PEG5k | 10 | 178 ± 2 | 0.10 | -5.3 ± 1.6 | 2.3 |
| PLGA + PLGA-PEG5k | 5 | 151 ± 13 | 0.07 | -9.0 ± 0.8 | 3.2 |
| PLA-PEG5k | 10 | 184 ± 9 | 0.10 | -6.0 ± 0.6 | 2.1 |
| PLA + PLA-PEG5k | 5 | 196 ± 13 | 0.06 | -8.2 ± 0.5 | 2.8 |

easured by dynamic

**Table 4.3.** Charaterization of biodegradable telmisartan nanoparticles produced by the zinc chelation method

| Zinc Chloride (mM) | Diameter[a] (nm) | PDI[a] | ζ-potential[b] (mV) | Drug loading (%) |
|---|---|---|---|---|
| 25 | 116 ± 2 | 0.07 | -6.4 ± 1.0 | 1.1 |
| 62.5 | 114 ± 3 | 0.08 | -7.5 ± 0.7 | 1.2 |
| 125 | 111 ± 3 | 0.08 | -12 ± 4 | 1.1 |
| 250 | 101 ± 3 | 0.09 | -9.6 ± 1.3 | 1.4 |

[a] Hydrodynamic diameter and polydispersity index (PDI) measured by dynamic light scattering.

[b] Measured in 10 mM NaCl at pH 7.4.

**Table 4.4.** Physicochemical properties of telmisatan nanocrystals

| Formulation | Size[a] (nm) | PDI[a] | Length[b] (nm) | Width[b] (nm) | ζ-potential[c] (mV) |
|---|---|---|---|---|---|
| F127/TEL-NC | 110 ± 7 | 0.2 | 180 ± 4 | 33 ± 1 | -2.0 ± 0.2 |
| F68/TEL-NC | 250 ± 50 | 0.2 | 280 ± 8 | 44 ± 1 | -5.0 ± 0.2 |
| TEL-FD | 1300 ± 50 | 0.4 | -- | -- | -- |

[a] Measured by dynamic light scattering.

[b] Measured from TEM images.

[c] Measured in 10 mM NaCl at pH 7.4.

# 5. Efficacy of telmisartan nanocrystals in COPD animal models

## *5.1 Introduction*

Chronic obstructive pulmonary disease (COPD) is currently the third leading cause of death in the United States [1] with continuously increasing mortality [2]. COPD is a progressive disease primarily caused by cigarette smoke (CS) as well as other inhaled pollutants [3]. The disease is characterized by chronic, irreversible obstruction of airflow from the lung, which is resulted from airspace enlargement (i.e. emphysema), as well as airway inflammation and remodeling [4]. Common symptoms of COPD are dyspnea, chronic cough, and sputum production [4]. Current treatment options fail to treat the underlying causes of disease and only provide symptom relief [10]. Smoking cessation influences the nature history of disease and is the most effective way to limit disease progression [11]. The primary pharmacological treatments for COPD are inhaled bronchodilators, such as β-agonists and muscarinic antagonists, and corticosteroids [4, 12]. Thus new therapeutic options that intervene in the natural history of the disease are sorely needed.

Appropriate preclinical models are critical to properly evaluate the effect of new therapeutics. There are multiple methods to generate COPD animal models, especially in mice, and these models are typically categorized as induced or genetic. CS exposure is the most widely studied induced model [89-91]. This is logical given that the primary risk factor for COPD development and progression in humans is tobacco smoke [3]. The COPD-like pathology is established by daily CS exposure for an extended period of time, typically weeks to months, either via whole body or nose-only exposure systems [90]. Mice exposed to chronic CS develop airspace enlargement, small airway remodeling,

chronic inflammation, and elevated oxidative stress [92]. However, a major limitation of the smoke exposure models is that regardless of the method parameters, the pathology of severe disease in humans cannot be replicated [89]. Specifically, while CS exposure can produce the emphysema phenotype and inflammation, mucus hypersecretion and airway obstruction are not established despite the presence of goblet cell metaplasia and airway remodeling [92]. A common genetic model is the tight skin (TSK) mouse which has a heterozygous duplication of the fibrilin-1 gene [94]. This mutation results in excess matrix deposition with fibrosis in the skin as well as impaired alveolar septation that progresses to airspace enlargement [96, 97]. This phenotype is at least partially attributed to cell death as a result of oxidative stress [98]. However, inflammation has not been implicated in the pathology [99].

Here, we have developed an inhalable nanocrystal (NC) formulation with the angiotensin receptor blocker (ARB) telmisartan (TEL; TEL-NC) for the localized treatment of COPD. We demonstrated that the inhalable nano-formulation enhanced the efficacy of TEL by improving lung drug levels over time compared with oral administration. We also anticipate that the inhalable ARB will allow for reduced dose and/or dosing frequency compared to the conventional oral dosage form. Our studies will ultimately provide proof-of-concept evidence that therapeutics targeting the TGF- β pathway can be reliably delivered by inhalation to the airway and airspace compartments in the lung, and intervene in pathological events observed in COPD.

## *5.2 Methods*

### *5.2.1 Animals*

All animal protocols were approved by the Institutional Animal Care and Use Committee at the Johns Hopkins Medical Institutions. All mice were allowed to acclimate for 1-2 weeks before handling, with access to food and water ad libitum throughout the experiments. Female C57/B6 6-8 weeks of age were obtained from Harlan. TSK mice were obtained from Jackson Laboratory (Bar Harbor, ME) and bred with C57/B6 wild type mice [98].

### *5.2.2 Formulation and characterization of F127/TEL-NC*

TEL and Pluronic F127 were dissolved in 2 ml of chloroform at a 1:4 mass ratio. The chloroform was rapidly evaporated with a nitrogen gas stream to create a film. The film was further dried via vacuum overnight. The film was hydrated with ultrapure water and incubated for 20 minutes at room temperature followed by bath sonication for 10 minutes. The suspension was further homogenized with a Vibra-Cell$^{TM}$ VCX-500 probe sonicator for 30 minutes with a pulse of 1 second on 1 second off at 100% amplitude. The resultant suspension was centrifuged at 2000 rpm for 5 minutes to remove any large particulates. F127/TEL-NC were collected via centrifugation at 21130x*g* for 10 minutes and were resuspended in ultrapure water. To measure TEL concentration, F127/TEL-NC were dissolved in methanol and the concentration was measured using a spectrofluorophotometer at excitation 300 and emission 360 nm with a slit width of 3 for both the excitation and emission. The TEL free drug (TEL-FD) was prepared by crushing Micardis® tablets into a powder and creating a suspension in water. The hydrodynamic

diameter of F127/TEL-NC in water was measured via dynamic light scattering (DLS) with a Zetasizer Nano ZS.

### *5.2.3 Pharmacokinetics*

C57/B6 mice were anesthetized with an intraperitoneal injection of avertin and administered 3 mg/kg of F127/TEL-NC or TEL-FD via intratracheal aspiration or TEL-FD via oral gavage. Mice were sacrificed and various time points and lungs and plasma were collected (n=5 per time point). To measure the TEL concentration in the lungs, the tissues were dried via lyophilzation and then crushed to a powder with a mortar and pestle. The drug was extracted into 1 ml of 50:50 methanol and DMSO at pH 3 and 200 µl of acetonitrile following homogenization with a bullet blender for 10 minutes. The samples were centrifuged at 21130x*g* for 10 minutes, the supernatant was collected and was diluted 10-fold with the methanol/DMSO solvent mixture. For the plasma samples, 0.2 ml of acetonitrile was added to precipitate the serum proteins. The samples were centrifuged at 21130x*g* for 10 minutes, the supernatant was collected and was diluted 10-fold with methanol/DMSO solvent mixture. The drug concentration in both lung and plasma samples was measured with a spectrofluorophotometer (Shimadzu) at an excitation of 300 and emission of 385 nm with a slit width of 3 for both excitation and emission.

### *5.2.4 Cigarette smoke exposure*

C57/B6 mice 6-8 weeks old were divided into three groups with 6 mice per group. Control mice were exposed to room air (RA) only. The animals exposed to CS were

either left untreated or were administered 1 mg/kg of F127/TEL-NC via intratracheal aspiration twice a week for a month concomitantly with the CS exposure. CS exposure was carried out (5 hours per day, 5 days per week) by burning 2R4F reference cigarettes (University of Kentucky, Louisville, Kentucky, USA) using a smoking machine (Model TE-10; Teague Enterprises). Cigarettes were smoked with standard puffs of 35 ml volume of 2-second duration. The average concentration of total suspended particulates and carbon monoxide was 90 mg/m$^3$ and 350 ppm, respectively, and was monitored on a daily basis [85, 178].

### *5.2.5 TSK model*

Treatment of TSK mice was initiated at 2 weeks of age. Mice were left untreated or administered 1 mg/kg of TEL-FD via oral gavage daily or 1 mg/kg of F127/TEL-NC via intratracheal aspiration twice a week for two weeks. Wild type (WT) litter mates were used as controls. All animals were sacrificed at 4 weeks of age except the control TSK group that was sacrificed at 2 weeks of age.

### *5.2.6 Morphometry*

For histologic and morphometric analyses, mouse lungs were inflated with agarose and fixed with 4% PFA. The lungs were equilibrated in cold 4% PFA overnight, sectioned, and then embedded in paraffin wax. Sections were cut at 5 μm and either stained with H&E or processed for immunohistochemistry. Mean linear intercept measurements were performed on H&E-stained sections taken at intervals throughout the lungs. Ten to fifteen images per slide were acquired at 20x magnification. Mean linear

intercepts were assessed by automated morphometry with a macro-operation performed by Metamorph Imaging Software (Universal Imaging, Molecular Devices).

### *5.2.7 Immunohistochemistry.*

Tissue sections were deparaffinized and rehydrated in an ethanol series. Antigens were retrieved by incubation in boiling citrate buffer (10 mM, pH 6.0) for 10 minutes. Sections were blocked for nonspecific binding with 3% normal serum from chicken and incubated with the primary antibodies for 1 hour at room temperature followed by incubation with the primary antibody overnight at 4°C. Slides were washed with phosphate buffered saline with Tween 20 (PBST). For phosphorylated Smad2 (pSmad2) staining, the pSmad2/3 antibody (Maine Medical Center Research Institute) was diluted 1:2000 and the staining was developed with the anti-rabbit UltraVision detection kit (Thermo Scientific). For 8-hydroxyguanosine (8-OHdG) staining, the antibody (Novus Biologicals) was diluted 1:200, incubated with the secondary antibody (Vector Laboratories), and staining was detected with the ABC system kit from Vector Laboratories. Quantitative immunohistochemistry was performed by normalizing staining to tissue area using Metamorph software. Images were captured with Nikon Elements on a Nikon Upright Biological Microscope Model Eclipse 80i.

### *5.2.8 Measurement of inflammatory cells*

Bronchial alveolar lavage fluid (BALF) was collected by washing the lungs with 1 ml of PBS three times. Cells were collected via centrifugation. The cells were fixed in PFA and were counted with a hemocytometer. Differential cell counting samples were

prepared as follows. Cells were fixed onto microscope slides via cytospins and allowed to dry overnight. The cells were stained with Diff-Quik stain. Cells were imaged with a Nikkon E-600 microscope and a total of 5-10 images were take per sample. A trained, blinded participant classified each cell in the images as macrophage, neutrophil, lymphocyte, or other. A minimum of 300 cells were classified per sample.

#### *5.2.9 Statistics*

Comparisons between multiple groups were determined using one-way analysis of variance (ANOVA) with Tukey's post hoc test. Calculations were performed using GraphPad Prism software. P values less than 0.05 were considered significant.

### ***5.3 Results***

#### *5.3.1 Pharmacokinetics*

A primary advantage of local drug delivery is to increase the drug exposure at the site of injury and potentially limit the systemic drug exposure. We hypothesized that the daily oral dosing regimen may not provide a therapeutically effective drug concentration in the lung, and that the inhaled F127/TEL-NC formulation would provide improved pulmonary drug concentration compared to systemically administered TEL-FD. We thus assessed the lung PK of inhaled F127/TEL-NC compared with that of TEL-FD administered via an oral gavage. Intratracheally administered TEL F127/TEL-NC significantly improved the local drug concentration over time up to 24 h compared to the orally administered TEL-FD (Figure 1A). The AUC from locally administered F127/TEL-NC was 4.6-fold greater than the oral gavage free drug TEL. Further, we

compared the lung PK of the F127/TEL-NC to intratracheally administered TEL-FD and found that the drug concentration from F127/TEL-NC was significantly higher at all time points with a 7–fold higher AUC. We also measured the drug plasma concentration of the oral TEL-FD, inhaled TEL-FD and inhaled F127/TEL-NC (Figure 1B). Interestingly, the initial plasma concentration of the intratracheally administered F127/TEL-NC was higher than that of the other two dosing schemes.

### *5.3.2 Protective effect of inhaled F127/TEL-NC in an acute model of CS-exposed lung injury*

We next investigated the effect of inhaled F127/TEL-NC in the lungs of an acute model of CS-exposure. Short term exposure (i.e. 4 weeks) of CS induced increased TGF-β signaling as indicated by the phosphorylation of the cytoplasmic signaling molecule Smad2 (pSmad2) (Figure 2A, 2B; $p < 0.05$) [85, 179]. Intratracheal administration of F127/TEL-NC (1 mg/kg TEL) twice per week for four weeks, concomitantly initiated with CS exposure, effectively suppressed the phosphorylation of Smad2 compared with CS only mice ($p < 0.05$); the pSmad2 level of F127/TEL-NC treated CS-exposed mice was comparable to that of RA control mice (Figure 2A, 2B). The enhanced 8-OHdG level indicates that oxidative stress was also elevated by an acute CS exposure (Figures 2C, 2D). Further, we confirmed that the acute CS exposure triggered immune cell infiltration, as evidenced by an increase in total inflammatory cells (Figure 3A, $p < 0.05$) and the fraction of neutrophils in BALF (Figure 3B, $p < 0.05$) compared to the RA control. We found that the acute CS-induced oxidative stress (Figures 2C, 2D) and lung inflammation (Figure 3) were both attenuated by concomitant intratracheal administration of F127/TEL-NC.

### *5.3.3 Therapeutic effect of inhaled F127/TEL-NC in a transgenic mouse model of emphysema*

We next investigated whether inhaled F127/TEL-NC is capable of therapeutically attenuating TGF-β signaling, and thus the subsequent pathological events. To do this, we utilized the TSK transgenic mouse model of emphysema. We initiated treatment of either daily oral administration of TEL-FD or four doses of intratracheal F127/TEL-NC at 2-weeks of age (when airway enlargement is evident; [98]) that lasted for 2 weeks, and lungs were harvested at 4-weeks of age. Following intratracheal administration of F127/TEL-NC partial reversal of airway enlargement was achieved based on histological analysis (Figure 4A). Quantitatively, the airspace diameter, as indicated by the mean linear intercept (MLI), was significantly reduced upon intratracheal treatment with F127/TEL-NC compared with the TSK mice evaluated at the same time point (Figure). Importantly, the MLI with F127/TEL-NC treatment was statistically lower than that at 2 weeks of age when dosing began.

We also confirmed that F127/TEL-NC significantly decreased the pSmad2 level in the lungs of TSK mice (Figure 4B), indicating TGF-β antagonism by the treatment. Additionally, the pSmad expression with F127/TEL-NC evaluated at 4 weeks was significantly reduced compared with that at 2 weeks of age when treatment was initiated. Further, inhaled F127/TEL-NC significantly reduced oxidative stress levels in the lung as indicated by enhanced 8-OHdG expression (Figure 4C). In contrast, we found that the daily oral TEL-FD had no effect on the airspace enlargement, the elevated pSmad2 expression, or the elevated oxidative stress.

### *5.4 Discussion*

There are currently no treatment options in the clinic or clinical trials that effectively halt progression or achieve reversal of COPD. The majority of the current pre-clinically tested treatments only show protection and not a therapeutic effect. Here, in addition to achieving protection in an acute CS model of lung injury, we also show a therapeutic reversal of lung damage in the transgenic TSK model following treatment with the inhaled F127/TEL-NC. This effect was only achieved with the inhaled nanocrystal formulation as opposed to the free drug administered orally.

COPD is a complex heterogeneous disease characterized by obstructed airflow due chronic inflammation and alveolar destruction. Thus, therapies to combat inflammation and/or induce tissue regeneration are currently being investigated. The reduction and/or elimination of inflammation is considered one of the primary approaches to prevent and potentially reverse disease progression [180]. A gamut of anti-inflammatory therapies targeting specific inflammatory mediators and oxidative stress as well as broad-spectrum inflammation are currently being extensively studied [181]. The basic pathophysiological and molecular mechanisms of the inflammation in COPD are still poorly understood, and thus pose a significant challenge to the discovery and development of new therapies to halt or reverse the progression of disease and ultimately reduce mortality [180]. Because of the significant risk in development of new agents, the repurposing of agents already approved for other indications is an attractive strategy.

Alternatively, strategies to regenerate destroyed tissue are being studied as well [182-184]. Recently, liver growth factor was shown to actually reverse airspace enlargement as well as ameliorate lung inflammation after establishment of emphysema

in a CS-exposure mouse model [185, 186]. Further, stem cell therapies are currently in clinical trials to treat COPD and preliminary results show improved lung function [187] and anti-inflammatory effects [188].

Here, we focus on the TFG-β pathway which has been implicated in the pathogenesis of COPD and has been shown to be elevated in the lungs of COPD patients. In particular, TGF-β dysregulation is associated with inflammation, oxidative stress, and cell death [85], and thus it is a very attractive target for COPD therapy. We previously showed that oral administration of the ARB losartan (LOS) effectively protected the lungs in a chronic CS-exposure model. Here, we expanded upon the prior work by repurposing TEL, another ARB that is FDA approved therapy for hypertension, to treat COPD and engineering an inhalable nano-formulation of TEL.

We first investigated the preventative effect of F127/TEL-NC in an acute CS exposure model. Although acute CS exposure is insufficient to develop the emphysema phenotype, we previously confirmed that only 2 weeks of exposure significantly increased the TGF-β levels in lung lysates [85]. Alternatively, the chronic CS-induced emphysema models typically take 4 to 6 months to establish [90]. Further, ARBs have typically been delivered orally either via gavage [189-191] or administered in food or water [192-194] as opposed to inhalation. Thus this shorter exposure model also allowed us to determine the appropriate dose for pulmonary delivery. Here we confirmed that four weeks (i.e acute) CS-exposure induced TGF-β signaling, thus validating the acute CS-exposed model to evaluate the TGF-β antagonizing effect of F127/TEL-NC. Further, enhanced TGF-β signaling increases reactive oxygen species [195] and can promote inflammation [196]. Both oxidative stress and inflammatory cells were elevated by the

acute CS-exposure. Intratracheal F127/TEL-NC attenuated the TGF-β expression as well as the oxidative stress and inflammation, thus suggesting that the local treatment effectively prevented TFG-b signaling in the lungs of an acute CS-exposed mouse model of lung injury.

Next we tested the therapeutic effect of F127/TEL-NC in the TSK transgenic model of emphysema. Compared with chronic CS-exposed models, the TSK mouse model develops early and extensive emphysema, a key pathological event in the airspace of COPD patients, and, thus serves as a rigorous model for testing therapeutic reversal of established emphysema [98, 197]. TGF-β signaling is elevated in TSK mice, suggesting that the airspace enlargement in the mouse model may be TGF-β-dependent [98, 198-200]. Further, increased oxidative stress, an effector pathway for TGF-β, contributes significantly to the airspace phenotype [98]. Thus this model was appropriate for preliminary studies of the therapeutic effect of F127/TEL-NC. Intratracheally administered F127/TEL-NC effectively suppressed TGF-β expression which manifested in attenuation of airspace enlargement and reduced levels of oxidative stress. On the other hand, daily oral TEL-FD at the same dose had no effect on the lung damage and oxidative stress. Importantly, inhaled F127/TEL-NC not only attenuated disease progression, but also demonstrated partial reversal of airspace enlargement and TGF-β expression at the end point compared with the initiation of treatment, indicating a therapeutic as opposed to preventative effect.

Daily oral treatment did not resolve lung damage in the TSK model likely because this conventional dosing regimen did not provide a sufficient local drug concentration required for therapeutic reversal of established lung injury. We achieved higher local

drug concentrations in the lung with intratracheal F127/TEL-NC compared with both oral and inhaled TEL-FD. This suggests that the dose and dosing frequency can be reduced with inhaled F127/TEL-NC, both of which are important for user compliance. Further, inhalation of the TEL-FD showed no pharmacokinetic improvement compared with oral free drug, which indicates that inhalation alone is not sufficient to achieve higher drug concentration in the lungs. TEL is very hydrophobic and thus the drug aggregates can be cleared via mucociliary and/or macrophage clearance [45].

### *5.5 Conclusion*

These findings suggest that intratracheally administered F127/TEL-NC, unlike oral daily free drug TEL-FD, can partially reverse pathologic airspace enlargement and also ameliorate lung injury caused by enhanced TGF-β signaling. These findings underscore that the conventional daily oral dosing regimen may not provide a local drug concentration required for therapeutic reversal of established COPD lung disease. In the future, we plan to investigate the therapeutic effect of F127/TEL-NC in a chronic model.

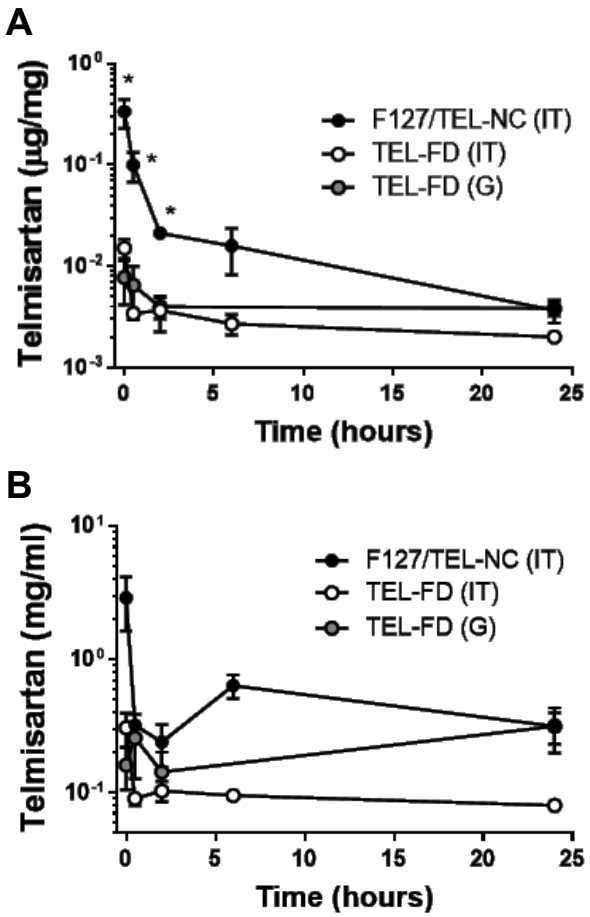


**Figure 5.1. Pharmacokinetics of telmisartan in mouse lung tissue and plasma.** The amount of TEL was measured in (A) the lung tissue and (B) the plasma over time following administration of F127/TEL-NC via inhalation (IT), TEL-FD administered via inhalation (IT), and TEL-FD administered via oral gavage (G). Data represents n = 5 mice per group. Error bars represent the standard error of the mean. *Denotes statistical significance ($p < 0.05$)

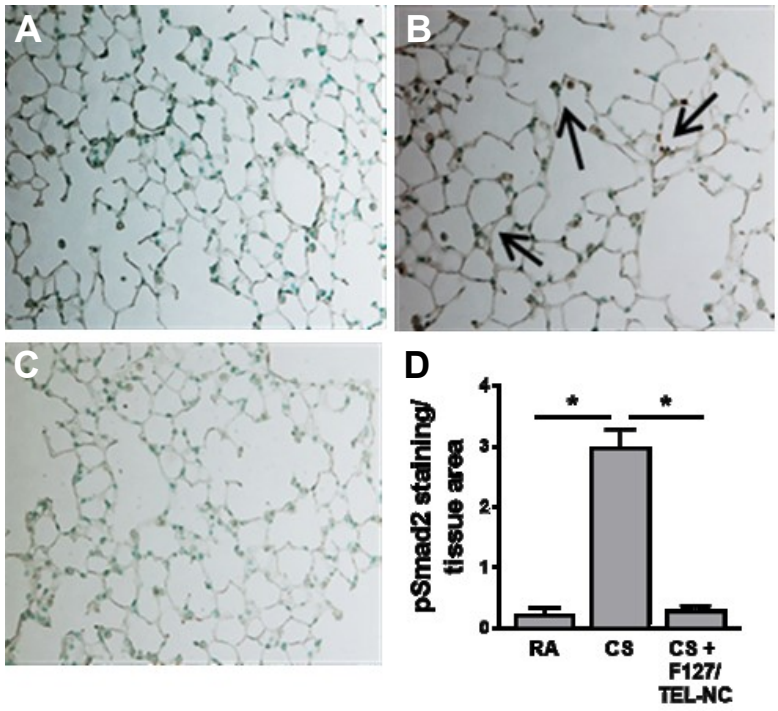


**Figure 5.2. Preventive effect of inhaled F127/TEL-NC in an acute model of cigarette smoke-exposed lung injury: TFG-b expression.** (A-C) Representative images of pSmad2 stained lung sections of mice exposed to (A) room air (RA), (B) cigarette smoke (CS), and (C) CS treated with inhaled temisartan nanocrystals (CS+F127/TEL-NC). (D) Quantification of pSmad2 staining. Data represents n = 6 mice per group. Error bars represent the standard error of the mean.*Denotes statistical significance compared to CS ($p < 0.05$)

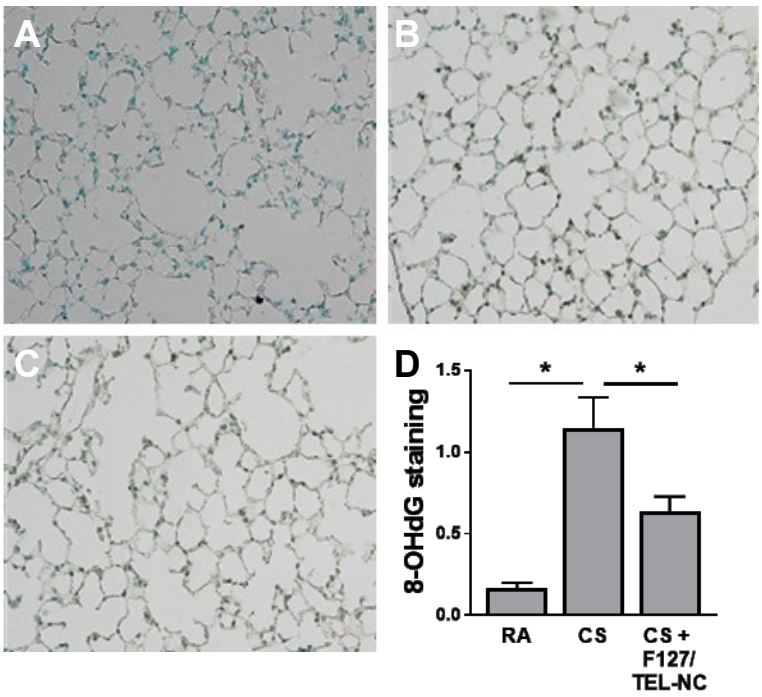


**Figure 5.3. Preventive effect of inhaled F127/TEL-NC in an acute model of cigarette smoke-exposed lung injury: oxidative stress.** (C) Representative images of 8-OHdG stained lung sections of mice exposed to (A) room air (RA), (B) cigarette smoke (CS), and (C) CS treated with inhaled temisartan nanocrystals (CS+F127/TEL-NC). (D) Quantification of 8-OHdG staining. *Denotes statistical significance compared to CS ($p < 0.05$)

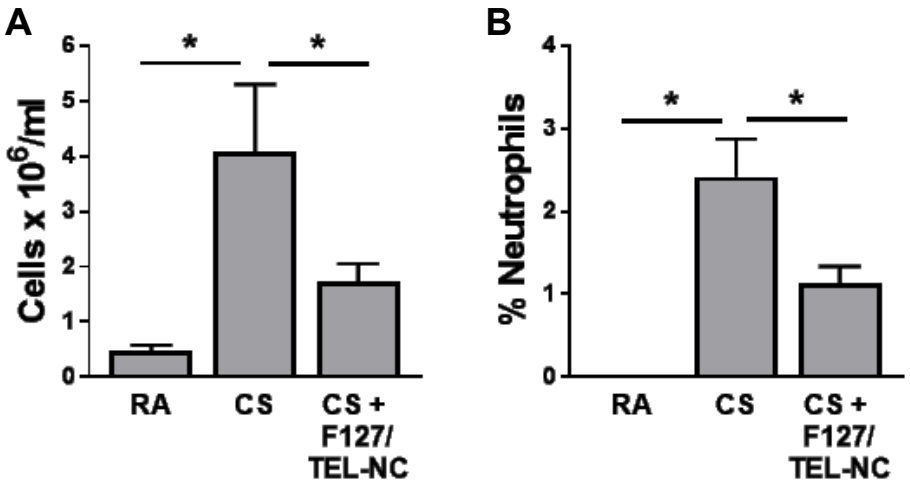


**Figure 5.4. Preventive effect of inhaled F127/TEL-NC in an acute model of cigarette smoke-exposed lung injury: inflammation.** (A) Total cell count in the BALF. (B) The percent of neutrophils in the BALF. Data represents n = 6 mice per group. Error bars represent the standard error of the mean. *Denotes statistical significance compared to CS ($p < 0.05$)

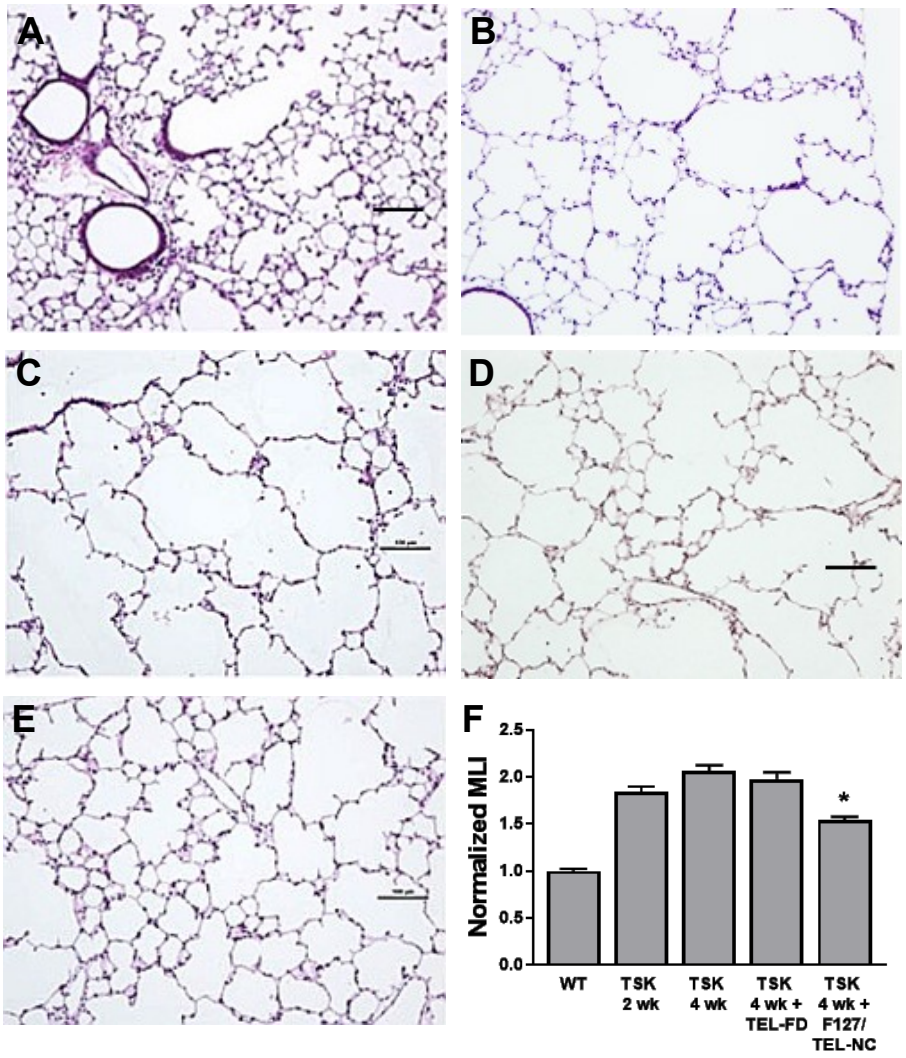


**Figure 5.5. Therapeutic effect of inhaled F127/TEL-NC in the transgenic TSK mouse model of emphysema: airspace enlargement.** (A-E) Representative images of H&E stained lung sections of (A) wild-type (WT), (B) TSK mice at 2 weeks (TSK 2wk), (C) TSK mice at 4 weeks (TSK 4wk), (D) TSK treated with daily oral gavage of free drug (TSK 4wk+TEL-FD), and (E) TSK treated with intratracheal drug nanocrystals (TSK 4wk+F127/TEL-NC). (F) Quantification of mean linear intercept (MLI). Error bars represent the standard error of the mean. *Denotes statistical significance compared to all other groups ($p < 0.05$)

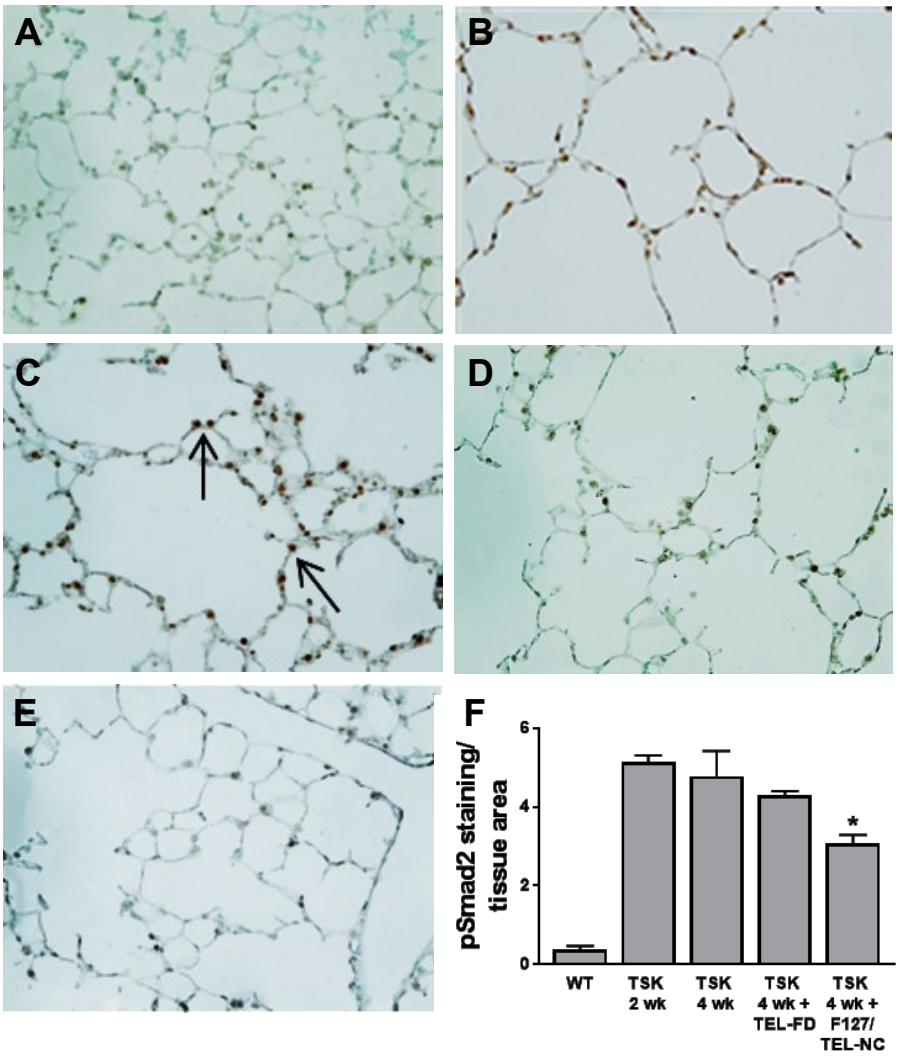


**Figure 5.6. Therapeutic effect of inhaled F127/TEL-NC in the transgenic TSK mouse model of emphysema: TGF-β expression.** (A-E) Representative images of pSmad2 stained lung sections of (A) wild-type (WT), (B) TSK mice at 2 weeks (TSK 2wk), (C) TSK mice at 4 weeks (TSK 4wk), (D) TSK treated with daily oral gavage of free drug (TSK 4wk+TEL-FD), and (E) TSK treated with intratracheal drug nanocrystals (TSK 4wk+F127/TEL-NC). (F) Quantification of pSmad2 staining. Error bars represent the standard error of the mean. *Denotes statistical significance compared to all other groups ($p < 0.05$)

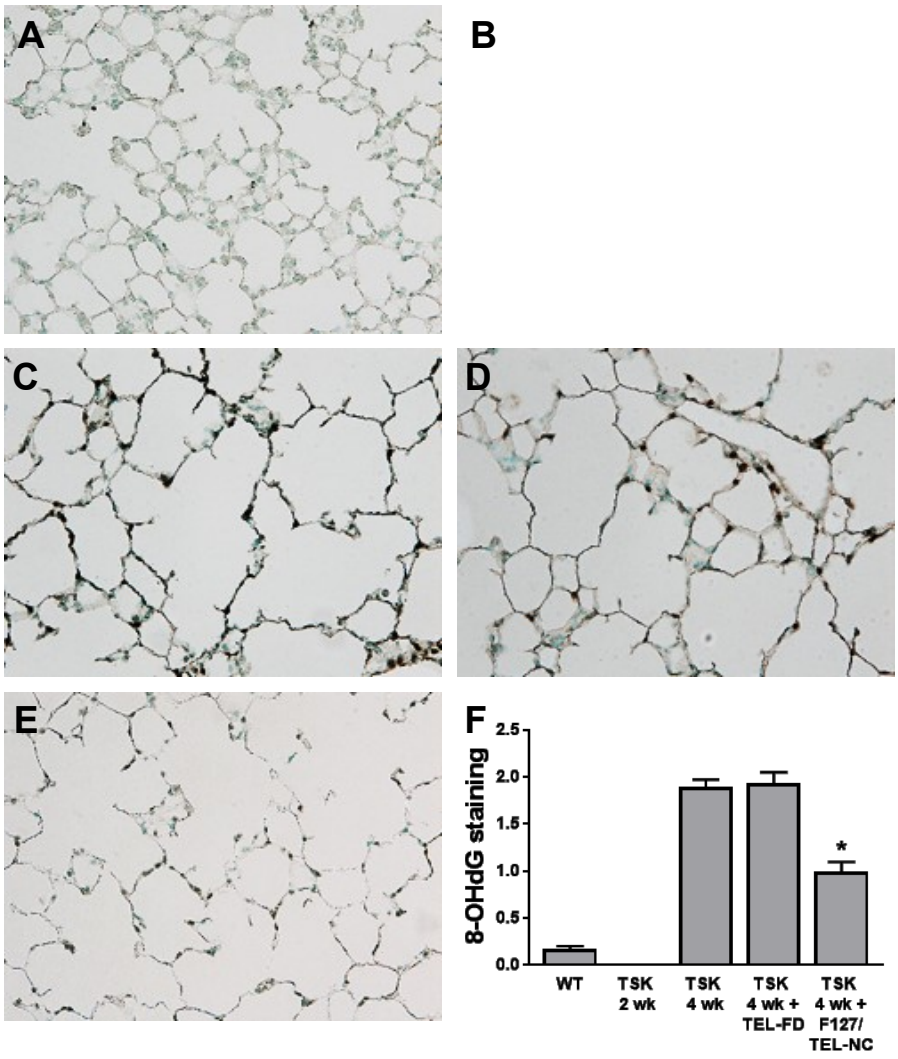


**Figure 5.7. Therapeutic effect of inhaled F127/TEL-NC in the transgenic TSK mouse model of emphysema: oxidative stress.** (A-E) Representative images of 8-OHdG stained lung sections of (A) wild-type (WT), (B) TSK mice at 2 weeks (TSK 2wk), (C) TSK mice at 4 weeks (TSK 4wk), (D) TSK treated with daily oral gavage of free drug (TSK 4wk+TEL-FD), and (E) TSK treated with intratracheal drug nanocrystals (TSK 4wk+F127/TEL-NC). (F) Quantification of 8-OHdG staining. Error bars represent the standard error of the mean. *Denotes statistical significance compared to all other groups ($p < 0.05$)

## References


1. Hoyert, D.L. and J. Xu, *Deaths: preliminary data for 2011.* Natl Vital Stat Rep, 2012. **61**(6): p. 1-51.
2. Lopez-Campos, J.L., W. Tan, and J.B. Soriano, *Global burden of COPD.* Respirology, 2016. **21**(1): p. 14-23.
3. Tuder, R.M. and I. Petrache, *Pathogenesis of chronic obstructive pulmonary disease.* J Clin Invest, 2012. **122**(8): p. 2749-55.
4. Vogelmeier, C.F., et al., *Global Strategy for the Diagnosis, Management, and Prevention of Chronic Obstructive Lung Disease 2017 Report. GOLD Executive Summary.* Am J Respir Crit Care Med, 2017. **195**(5): p. 557-582.
5. Buist, A.S., et al., *International variation in the prevalence of COPD (the BOLD Study): a population-based prevalence study.* Lancet, 2007. **370**(9589): p. 741-50.
6. Bestall, J.C., et al., *Usefulness of the Medical Research Council (MRC) dyspnoea scale as a measure of disability in patients with chronic obstructive pulmonary disease.* Thorax, 1999. **54**(7): p. 581-6.
7. Guyatt, G.H., et al., *A measure of quality of life for clinical trials in chronic lung disease.* Thorax, 1987. **42**(10): p. 773-8.
8. Jones, P.W., et al., *A self-complete measure of health status for chronic airflow limitation. The St. George's Respiratory Questionnaire.* Am Rev Respir Dis, 1992. **145**(6): p. 1321-7.
9. *Diagnosing COPD*, in *Chronic Obstructive Pulmonary Disease: Management of Chronic Obstructive Pulmonary Disease in Adults in Primary and Secondary Care*2010, Royal College of Physicians (UK): London.

10. Martinez, F.J., J.F. Donohue, and S.I. Rennard, *The future of chronic obstructive pulmonary disease treatment--difficulties of and barriers to drug development.* Lancet, 2011. **378**(9795): p. 1027-37.

11. van Eerd, E.A., et al., *Smoking cessation for people with chronic obstructive pulmonary disease.* Cochrane Database Syst Rev, 2016(8): p. CD010744.

12. Ross, C.L. and T.T. Hansel, *New drug therapies for COPD.* Clin Chest Med, 2014. **35**(1): p. 219-39.

13. Ejiofor, S. and A.M. Turner, *Pharmacotherapies for COPD.* Clin Med Insights Circ Respir Pulm Med, 2013. **7**: p. 17-34.

14. DeCamp, M.M., Jr., et al., *The evaluation and preparation of the patient for lung volume reduction surgery.* Proc Am Thorac Soc, 2008. **5**(4): p. 427-31.

15. Cone, R.A., *Barrier properties of mucus.* Adv Drug Deliv Rev, 2009. **61**(2): p. 75-85.

16. Cone, R., *Mucus*, in *Mucosal Immunlogy*, W.S. Michael E. Lamm, Jerry R. McGhee, Lloyd Mayer, Jiri Mestecky, John Bienenstock, Editor 1999, Academic Press: San Diego. p. 43-64.

17. Knowles, M.R. and R.C. Boucher, *Mucus clearance as a primary innate defense mechanism for mammalian airways.* J Clin Invest, 2002. **109**(5): p. 571-7.

18. Jeffery, P.K. and D. Li, *Airway mucosa: secretory cells, mucus and mucin genes.* Eur Respir J, 1997. **10**(7): p. 1655-62.

19. Williams, O.W., et al., *Airway mucus: From production to secretion.* Am J Respir Cell Mol Biol, 2006. **34**(5): p. 527-36.

20. Ramos, F.L., J.S. Krahnke, and V. Kim, *Clinical issues of mucus accumulation in COPD.* Int J Chron Obstruct Pulmon Dis, 2014. **9**: p. 139-50.

21. Caramori, G., et al., *Mucin expression in peripheral airways of patients with chronic obstructive pulmonary disease.* Histopathology, 2004. **45**(5): p. 477-84.

22. Saetta, M., et al., *Goblet cell hyperplasia and epithelial inflammation in peripheral airways of smokers with both symptoms of chronic bronchitis and chronic airflow limitation.* Am J Respir Crit Care Med, 2000. **161**(3 Pt 1): p. 1016-21.

23. Verra, F., et al., *Ciliary abnormalities in bronchial epithelium of smokers, ex-smokers, and nonsmokers.* Am J Respir Crit Care Med, 1995. **151**(3 Pt 1): p. 630-4.

24. King, M., *Physiology of mucus clearance.* Paediatr Respir Rev, 2006. **7 Suppl 1**: p. S212-4.

25. Hogg, J.C., et al., *Survival after lung volume reduction in chronic obstructive pulmonary disease: insights from small airway pathology.* Am J Respir Crit Care Med, 2007. **176**(5): p. 454-9.

26. Auerbach, O., E.C. Hammond, and L. Garfinkel, *Changes in bronchial epithelium in relation to cigarette smoking, 1955-1960 vs. 1970-1977.* N Engl J Med, 1979. **300**(8): p. 381-5.

27. Ebert, R.V. and M.J. Terracio, *The bronchiolar epithelium in cigarette smokers. Observations with the scanning electron microscope.* Am Rev Respir Dis, 1975. **111**(1): p. 4-11.

28. Holtzman, M.J., et al., *Acute and chronic airway responses to viral infection: implications for asthma and chronic obstructive pulmonary disease.* Proc Am Thorac Soc, 2005. **2**(2): p. 132-40.

29. Burgel, P.R. and J.A. Nadel, *Roles of epidermal growth factor receptor activation in epithelial cell repair and mucin production in airway epithelium.* Thorax, 2004. **59**(11): p. 992-6.

30. Innes, A.L., et al., *Epithelial mucin stores are increased in the large airways of smokers with airflow obstruction.* Chest, 2006. **130**(4): p. 1102-8.

31. Allinson, J.P., et al., *The Presence of Chronic Mucus Hypersecretion Across Adult Life in Relation to COPD Development.* Am J Respir Crit Care Med, 2015.

32. Vestbo, J., E. Prescott, and P. Lange, *Association of chronic mucus hypersecretion with FEV1 decline and chronic obstructive pulmonary disease morbidity. Copenhagen City Heart Study Group.* Am J Respir Crit Care Med, 1996. **153**(5): p. 1530-5.

33. Ekberg-Aronsson, M., et al., *Mortality in GOLD stages of COPD and its dependence on symptoms of chronic bronchitis.* Respir Res, 2005. **6**: p. 98.

34. Randell, S.H. and R.C. Boucher, *Effective mucus clearance is essential for respiratory health.* Am J Respir Cell Mol Biol, 2006. **35**(1): p. 20-8.

35. Hill, D.B., et al., *A biophysical basis for mucus solids concentration as a candidate biomarker for airways disease.* PLoS One, 2014. **9**(2): p. e87681.

36. Anderson, W.H., et al., *The Relationship of Mucus Concentration (Hydration) to Mucus Osmotic Pressure and Transport in Chronic Bronchitis.* Am J Respir Crit Care Med, 2015.

37. Kesimer, M., et al., *Airway Mucin Concentration as a Marker of Chronic Bronchitis.* N Engl J Med, 2017. **377**(10): p. 911-922.

38. Giordano, A.M., D. Holsclaw, and M. Litt, *Mucus rheology and mucociliary clearance: Normal physiologic state.* Am Rev Respir Dis, 1978. **118**(2): p. 245-50.

39. Serisier, D.J., et al., *Macrorheology of cystic fibrosis, chronic obstructive pulmonary disease & normal sputum.* Respir Res, 2009. **10**: p. 63.

40. Patton, J.S. and P.R. Byron, *Inhaling medicines: delivering drugs to the body through the lungs.* Nat Rev Drug Discov, 2007. **6**(1): p. 67-74.

41. Patton, J.S., C.S. Fishburn, and J.G. Weers, *The lungs as a portal of entry for systemic drug delivery.* Proc Am Thorac Soc, 2004. **1**(4): p. 338-44.

42. Rubin, B.K., *Pediatric aerosol therapy: new devices and new drugs.* Respir Care, 2011. **56**(9): p. 1411-21; discussion 1421-3.

43. Rubin, B.K., *Air and soul: the science and application of aerosol therapy.* Respir Care, 2010. **55**(7): p. 911-21.

44. Zhang, J., et al., *Formation, characterization, and fate of inhaled drug nanoparticles.* Adv Drug Deliv Rev, 2011. **63**(6): p. 441-55.

45. Labiris, N.R. and M.B. Dolovich, *Pulmonary drug delivery. Part I: physiological factors affecting therapeutic effectiveness of aerosolized medications.* Br J Clin Pharmacol, 2003. **56**(6): p. 588-99.

46. Winkler, J., G. Hochhaus, and H. Derendorf, *How the lung handles drugs: pharmacokinetics and pharmacodynamics of inhaled corticosteroids.* Proc Am Thorac Soc, 2004. **1**(4): p. 356-63.

47. Kurmi, B.D., et al., *Micro- and nanocarrier-mediated lung targeting.* Expert Opin Drug Deliv, 2010. **7**(7): p. 781-94.

48. Byron, P.R., *Prediction of drug residence times in regions of the human respiratory tract following aerosol inhalation.* J Pharm Sci, 1986. **75**(5): p. 433-8.

49. Langer, R., *Drug delivery and targeting.* Nature, 1998. **392**(6679): p. 5-10.

50. Farokhzad, O.C. and R. Langer, *Nanomedicine: developing smarter therapeutic and diagnostic modalities.* Adv Drug Deliv Rev, 2006. **58**(14): p. 1456-9.

51. Panyam, J. and V. Labhasetwar, *Biodegradable nanoparticles for drug and gene delivery to cells and tissue.* Adv Drug Deliv Rev, 2003. **55**(3): p. 329-47.

52. Allemann, E., J. Leroux, and R. Gurny, *Polymeric nano- and microparticles for the oral delivery of peptides and peptidomimetics.* Adv Drug Deliv Rev, 1998. **34**(2-3): p. 171-189.

53. Kwong, B., H. Liu, and D.J. Irvine, *Induction of potent anti-tumor responses while eliminating systemic side effects via liposome-anchored combinatorial immunotherapy.* Biomaterials, 2011. **32**(22): p. 5134-47.

54. Kim, Y.T., J.M. Caldwell, and R.V. Bellamkonda, *Nanoparticle-mediated local delivery of methylprednisolone after spinal cord injury.* Biomaterials, 2009. **30**(13): p. 2582-2590.

55. MacKay, J.A., D.F. Deen, and F.C. Szoka, Jr., *Distribution in brain of liposomes after convection enhanced delivery; modulation by particle charge, particle diameter, and presence of steric coating.* Brain Res, 2005. **1035**(2): p. 139-53.

56. Lai, S.K., et al., *Privileged delivery of polymer nanoparticles to the perinuclear region of live cells via a non-clathrin, non-degradative pathway.* Biomaterials, 2007. **28**(18): p. 2876-84.

57. Yuan, F., et al., *Microvascular permeability and interstitial penetration of sterically stabilized (stealth) liposomes in a human tumor xenograft.* Cancer Res, 1994. **54**(13): p. 3352-6.

58. Prego, C., et al., *Transmucosal macromolecular drug delivery.* Journal of Controlled Release, 2005. **101**(1-3): p. 151-62.

59. Medina-Kauwe, L.K., J. Xie, and S. Hamm-Alvarez, *Intracellular trafficking of nonviral vectors.* Gene Ther, 2005. **12**(24): p. 1734-51.

60. Astete, C.E. and C.M. Sabliov, *Synthesis and characterization of PLGA nanoparticles.* J Biomater Sci Polym Ed, 2006. **17**(3): p. 247-89.

61. Vert, M., J. Mauduit, and S. Li, *Biodegradation of PLA/GA polymers: increasing complexity.* Biomaterials, 1994. **15**(15): p. 1209-13.

62. Lai, S.K., et al., *Rapid transport of large polymeric nanoparticles in fresh undiluted human mucus.* Proc Natl Acad Sci U S A, 2007. **104**(5): p. 1482-7.

63. Suk, J.S., et al., *The penetration of fresh undiluted sputum expectorated by cystic fibrosis patients by non-adhesive polymer nanoparticles.* Biomaterials, 2009. **30**(13): p. 2591-7.

64. Schuster, B.S., et al., *Nanoparticle diffusion in respiratory mucus from humans without lung disease.* Biomaterials, 2013. **34**(13): p. 3439-46.

65. Lai, S.K., et al., *Drug carrier nanoparticles that penetrate human chronic rhinosinusitis mucus.* Biomaterials, 2011. **32**(26): p. 6285-90.

66. Duncan, G.A., et al., *Microstructural alterations of sputum in cystic fibrosis lung disease.* JCI Insight, 2016. **1**(18): p. e88198.

67. Schuster, B.S., et al., *Particle tracking in drug and gene delivery research: State-of-the-art applications and methods.* Adv Drug Deliv Rev, 2015.

68. Suk, J.S., et al., *Rapid transport of muco-inert nanoparticles in cystic fibrosis sputum treated with N-acetyl cysteine.* Nanomedicine (Lond), 2011. **6**(2): p. 365-75.

69. Suk, J.S., et al., *PEGylation as a strategy for improving nanoparticle-based drug and gene delivery.* Adv Drug Deliv Rev, 2016. **99**(Pt A): p. 28-51.

70. Schneider, C.S., et al., *Nanoparticles that do not adhere to mucus provide uniform and long-lasting drug delivery to airways following inhalation.* Sci Adv, 2017. **3**(4): p. e1601556.

71. Mastorakos, P., et al., *Highly compacted biodegradable DNA nanoparticles capable of overcoming the mucus barrier for inhaled lung gene therapy.* Proc Natl Acad Sci U S A, 2015. **112**(28): p. 8720-5.

72. Suk, J.S., et al., *Lung gene therapy with highly compacted DNA nanoparticles that overcome the mucus barrier.* J Control Release, 2014. **178**: p. 8-17.

73. Chen, H., et al., *Nanonization strategies for poorly water-soluble drugs.* Drug Discov Today, 2011. **16**(7-8): p. 354-60.

74. Shegokar, R. and R.H. Muller, *Nanocrystals: industrially feasible multifunctional formulation technology for poorly soluble actives.* Int J Pharm, 2010. **399**(1-2): p. 129-39.

75. Rabinow, B., *Pharmacokinetics of drugs administered in nanosuspension.* Discov Med, 2005. **5**(25): p. 74-9.

76. Junghanns, J.U. and R.H. Muller, *Nanocrystal technology, drug delivery and clinical applications.* Int J Nanomedicine, 2008. **3**(3): p. 295-309.

77. Gao, L., et al., *Drug nanocrystals: In vivo performances.* J Control Release, 2012. **160**(3): p. 418-30.

78. Yu, T., et al., *Mucus-Penetrating Nanosuspensions for Enhanced Delivery of Poorly Soluble Drugs to Mucosal Surfaces.* Adv Healthc Mater, 2016. **5**(21): p. 2745-2750.

79. Kabanov, A.V., et al., *Pluronic block copolymers: novel functional molecules for gene therapy.* Adv Drug Deliv Rev, 2002. **54**(2): p. 223-33.

80. ten Dijke, P. and C.S. Hill, *New insights into TGF-beta-Smad signalling.* Trends Biochem Sci, 2004. **29**(5): p. 265-73.

81. Kim, I.Y., M.M. Kim, and S.J. Kim, *Transforming growth factor-beta : biology and clinical relevance.* J Biochem Mol Biol, 2005. **38**(1): p. 1-8.

82. Bartram, U. and C.P. Speer, *The role of transforming growth factor beta in lung development and disease.* Chest, 2004. **125**(2): p. 754-65.

83. Santibanez, J.F., M. Quintanilla, and C. Bernabeu, *TGF-beta/TGF-beta receptor system and its role in physiological and pathological conditions.* Clin Sci (Lond), 2011. **121**(6): p. 233-51.

84. Krimmer, D.I., et al., *Matrix proteins from smoke-exposed fibroblasts are pro-proliferative.* Am J Respir Cell Mol Biol, 2012. **46**(1): p. 34-9.

85. Podowski, M., et al., *Angiotensin receptor blockade attenuates cigarette smoke-induced lung injury and rescues lung architecture in mice.* J Clin Invest, 2012. **122**(1): p. 229-40.

86. Sharafkhaneh, A., N.A. Hanania, and V. Kim, *Pathogenesis of emphysema: from the bench to the bedside.* Proc Am Thorac Soc, 2008. **5**(4): p. 475-7.

87. Jiang, F., et al., *NADPH oxidase-dependent redox signaling in TGF-beta-mediated fibrotic responses.* Redox Biol, 2014. **2**: p. 267-72.

88. Yang, Y., et al., *Transforming growth factor-beta 1 pathways in inflammatory airway diseases.* Allergy, 2014. **69**(6): p. 699-707.

89. Wright, J.L., M. Cosio, and A. Churg, *Animal models of chronic obstructive pulmonary disease.* Am J Physiol Lung Cell Mol Physiol, 2008. **295**(1): p. L1-15.

90. Churg, A., M. Cosio, and J.L. Wright, *Mechanisms of cigarette smoke-induced COPD: insights from animal models.* Am J Physiol Lung Cell Mol Physiol, 2008. **294**(4): p. L612-31.

91. Ghorani, V., et al., *Experimental animal models for COPD: a methodological review.* Tob Induc Dis, 2017. **15**: p. 25.

92. Vlahos, R. and S. Bozinovski, *Recent advances in pre-clinical mouse models of COPD.* Clin Sci (Lond), 2014. **126**(4): p. 253-65.

93. Tuder, R.M., S. McGrath, and E. Neptune, *The pathobiological mechanisms of emphysema models: what do they have in common?* Pulm Pharmacol Ther, 2003. **16**(2): p. 67-78.

94. Siracusa, L.D., et al., *A tandem duplication within the fibrillin 1 gene is associated with the mouse tight skin mutation.* Genome Res, 1996. **6**(4): p. 300-13.

95. Visconti, R.P., et al., *Codistribution analysis of elastin and related fibrillar proteins in early vertebrate development.* Matrix Biol, 2003. **22**(2): p. 109-21.

96. Martorana, P.A., et al., *A 16-month study of the development of genetic emphysema in tight-skin mice.* Am Rev Respir Dis, 1989. **139**(1): p. 226-32.

97. Rossi, G.A., et al., *Hereditary emphysema in the tight-skin mouse. Evaluation of pathogenesis.* Am Rev Respir Dis, 1984. **129**(5): p. 850-5.

98. Podowski, M., et al., *Complex integration of matrix, oxidative stress, and apoptosis in genetic emphysema.* Am J Pathol, 2009. **175**(1): p. 84-96.

99. Ito, S., et al., *Early emphysema in the tight skin and pallid mice: roles of microfibril-associated glycoproteins, collagen, and mechanical forces.* Am J Respir Cell Mol Biol, 2006. **34**(6): p. 688-94.

100. Rogers, D.F., *Mucus hypersecretion in chronic obstructive pulmonary disease.* Novartis Found Symp, 2001. **234**: p. 65-77; discussion 77-83.

101. Cerveri, I. and V. Brusasco, *Revisited role for mucus hypersecretion in the pathogenesis of COPD.* Eur Respir Rev, 2010. **19**(116): p. 109-12.

102. Kreda, S.M., C.W. Davis, and M.C. Rose, *CFTR, mucins, and mucus obstruction in cystic fibrosis.* Cold Spring Harb Perspect Med, 2012. **2**(9): p. a009589.

103. Evans, C.M., et al., *Mucus hypersecretion in asthma: causes and effects.* Curr Opin Pulm Med, 2009. **15**(1): p. 4-11.

104. Kim, V., et al., *The chronic bronchitic phenotype of COPD: an analysis of the COPDGene Study.* Chest, 2011. **140**(3): p. 626-33.

105. Marsh, S.E., et al., *Proportional classifications of COPD phenotypes.* Thorax, 2008. **63**(9): p. 761-7.

106. Fahy, J.V. and B.F. Dickey, *Airway mucus function and dysfunction.* N Engl J Med, 2010. **363**(23): p. 2233-47.

107. Danahay, H. and A.D. Jackson, *Epithelial mucus-hypersecretion and respiratory disease.* Curr Drug Targets Inflamm Allergy, 2005. **4**(6): p. 651-64.

108. Hogg, J.C., et al., *The nature of small-airway obstruction in chronic obstructive pulmonary disease.* N Engl J Med, 2004. **350**(26): p. 2645-53.

109. Burgel, P.R., et al., *Cough and sputum production are associated with frequent exacerbations and hospitalizations in COPD subjects.* Chest, 2009. **135**(4): p. 975-82.

110. Corhay, J.L., et al., *Chronic bronchitis in COPD patients is associated with increased risk of exacerbations: a cross-sectional multicentre study.* Int J Clin Pract, 2013. **67**(12): p. 1294-301.

111. Hurst, J.R., et al., *Susceptibility to exacerbation in chronic obstructive pulmonary disease.* N Engl J Med, 2010. **363**(12): p. 1128-38.

112. Lai, S.K., et al., *Micro- and macrorheology of mucus.* Adv Drug Deliv Rev, 2009. **61**(2): p. 86-100.

113. Xu, Q., et al., *Nanoparticle diffusion in, and microrheology of, the bovine vitreous ex vivo.* J Control Release, 2013. **167**(1): p. 76-84.

114. Nance, E.A., et al., *A dense poly(ethylene glycol) coating improves penetration of large polymeric nanoparticles within brain tissue.* Science Translational Medicine, 2012. **4**(149): p. 149ra119.

115. Nance, E., et al., *Brain-penetrating nanoparticles improve paclitaxel efficacy in malignant glioma following local administration.* ACS Nano, 2014. **8**(10): p. 10655-64.

116. Chisholm, J., et al., *Nanoparticle Diffusion In Sputum As A Biomarker Of COPD Severity*, in *A44. BIOMARKERS IN CHRONIC OBSTRUCTIVE PULMONARY DISEASE*2013, American Thoracic Society. p. A1514-A1514.

117. Couper, D., et al., *Design of the Subpopulations and Intermediate Outcomes in COPD Study (SPIROMICS).* Thorax, 2014. **69**(5): p. 491-4.

118. Schuster, B.S., et al., *Overcoming the cystic fibrosis barrier to leading adeno-associated virus gene therapy vectors.* Molecular Therapy, 2014. **in press**.

119. Schuster, B.S., et al., *Overcoming the cystic fibrosis sputum barrier to leading adeno-associated virus gene therapy vectors.* Molecular Therapy, 2014. **22**(8): p. 1484-93.

120. Suh, J., M. Dawson, and J. Hanes, *Real-time multiple-particle tracking: applications to drug and gene delivery.* Adv Drug Deliv Rev, 2005. **57**(1): p. 63-78.

121. Feinstein, A.R., *Principles of Medical Statistics*2001: Chapman and Hall/CRC.

122. Kim, A.J., et al., *Use of single-site-functionalized PEG dendrons to prepare gene vectors that penetrate human mucus barriers.* Angew Chem Int Ed Engl, 2013. **52**(14): p. 3985-8.

123. Sanders, N.N., et al., *Cystic fibrosis sputum: a barrier to the transport of nanospheres.* Am J Respir Crit Care Med, 2000. **162**(5): p. 1905-11.

124. Crowther, R.S. and R.F. Wetmore, *Fluorometric assay of O-linked glycoproteins by reaction with 2-cyanoacetamide.* Anal Biochem, 1987. **163**(1): p. 170-4.

125. Matsui, H., et al., *Reduced three-dimensional motility in dehydrated airway mucus prevents neutrophil capture and killing bacteria on airway epithelial surfaces.* J Immunol, 2005. **175**(2): p. 1090-9.

126. Bansil, R., et al., *The Influence of Mucus Microstructure and Rheology in Helicobacter pylori Infection.* Front Immunol, 2013. **4**: p. 310.

127. Ramsey, S.D. and F.D. Hobbs, *Chronic obstructive pulmonary disease, risk factors, and outcome trials: comparisons with cardiovascular disease.* Proc Am Thorac Soc, 2006. **3**(7): p. 635-40.

128. Paone, G., et al., *Analysis of sputum markers in the evaluation of lung inflammation and functional impairment in symptomatic smokers and COPD patients.* Dis Markers, 2011. **31**(2): p. 91-100.

129. Bartoli, M.L., et al., *Biological markers in induced sputum of patients with different phenotypes of chronic airway obstruction.* Respiration, 2009. **77**(3): p. 265-72.

130. Ensign, L.M., et al., *Mucus Penetrating Nanoparticles: Biophysical Tool and Method of Drug and Gene Delivery.* Advanced Materials, 2012. **24**(28): p. 3887-3894.

131. Mason, T.G., et al., *Particle tracking microrheology of complex fluids.* Physical Review Letters, 1997. **79**(17): p. 3282-3285.

132. Hauber, H.P., S.C. Foley, and Q. Hamid, *Mucin overproduction in chronic inflammatory lung disease.* Can Respir J, 2006. **13**(6): p. 327-35.

133. Wright, T.K., et al., *Neutrophil extracellular traps are associated with inflammation in chronic airway disease.* Respirology, 2016. **21**(3): p. 467-75.

134. Yuan, S., et al., *Oxidation increases mucin polymer cross-links to stiffen airway mucus gels.* Science Translational Medicine, 2015. **7**(276): p. 276ra27.

135. Nielsen, H., et al., *Elastic contributions dominate the viscoelastic properties of sputum from cystic fibrosis patients.* Biophys Chem, 2004. **112**(2-3): p. 193-200.

136. Repine, J.E., A. Bast, and I. Lankhorst, *Oxidative stress in chronic obstructive pulmonary disease. Oxidative Stress Study Group.* Am J Respir Crit Care Med, 1997. **156**(2 Pt 1): p. 341-57.

137. Kirkham, P.A. and P.J. Barnes, *Oxidative stress in COPD.* Chest, 2013. **144**(1): p. 266-73.

138. Tomaiuolo, G., et al., *A new method to improve the clinical evaluation of cystic fibrosis patients by mucus viscoelastic properties.* PLoS One, 2014. **9**(1): p. e82297.

139. Braga, P.C., et al., *Identification of subpopulations of bronchitic patients for suitable therapy by a dynamic rheological test.* Int J Clin Pharmacol Res, 1989. **9**(3): p. 175-82.

140. Papp, M., et al., *Angiotensin receptor subtype AT(1) mediates alveolar epithelial cell apoptosis in response to ANG II.* Am J Physiol Lung Cell Mol Physiol, 2002. **282**(4): p. L713-8.

141. Wong, M.H., O.C. Chapin, and M.D. Johnson, *LPS-stimulated cytokine production in type I cells is modulated by the renin-angiotensin system.* Am J Respir Cell Mol Biol, 2012. **46**(5): p. 641-50.

142. Marshall, R.P., R.J. McAnulty, and G.J. Laurent, *Angiotensin II is mitogenic for human lung fibroblasts via activation of the type 1 receptor.* Am J Respir Crit Care Med, 2000. **161**(6): p. 1999-2004.

143. Uhal, B.D., et al., *Angiotensin-TGF-beta 1 crosstalk in human idiopathic pulmonary fibrosis: autocrine mechanisms in myofibroblasts and macrophages.* Curr Pharm Des, 2007. **13**(12): p. 1247-56.

144. Molteni, A., et al., *Effect of an angiotensin II receptor blocker and two angiotensin converting enzyme inhibitors on transforming growth factor-beta (TGF-beta) and alpha-actomyosin (alpha SMA), important mediators of radiation-induced pneumopathy and lung fibrosis.* Curr Pharm Des, 2007. **13**(13): p. 1307-16.

145. Zhou, Y., et al., *Thrombospondin 1 mediates angiotensin II induction of TGF-beta activation by cardiac and renal cells under both high and low glucose conditions.* Biochem Biophys Res Commun, 2006. **339**(2): p. 633-41.

146. Kagami, S., et al., *Angiotensin II stimulates extracellular matrix protein synthesis through induction of transforming growth factor-beta expression in rat glomerular mesangial cells.* J Clin Invest, 1994. **93**(6): p. 2431-7.

147. Israili, Z.H., *Clinical pharmacokinetics of angiotensin II (AT1) receptor blockers in hypertension.* J Hum Hypertens, 2000. **14 Suppl 1**: p. S73-86.

148. Lo, M.W., et al., *Pharmacokinetics of losartan, an angiotensin II receptor antagonist, and its active metabolite EXP3174 in humans.* Clin Pharmacol Ther, 1995. **58**(6): p. 641-9.

149. Michel, M.C., et al., *A systematic comparison of the properties of clinically used angiotensin II type 1 receptor antagonists.* Pharmacol Rev, 2013. **65**(2): p. 809-48.

150. Shimoda, L.A., et al., *L-type Ca(2+) channels, resting [Ca(2+)](i), and ET-1-induced responses in chronically hypoxic pulmonary myocytes.* Am J Physiol Lung Cell Mol Physiol, 2000. **279**(5): p. L884-94.

151. Suresh, K., et al., *Hydrogen peroxide-induced calcium influx in lung microvascular endothelial cells involves TRPV4.* Am J Physiol Lung Cell Mol Physiol, 2015. **309**(12): p. L1467-77.

152. Seluanov, A., A. Vaidya, and V. Gorbunova, *Establishing primary adult fibroblast cultures from rodents.* J Vis Exp, 2010(44).

153. Xu, Q., et al., *Scalable method to produce biodegradable nanoparticles that rapidly penetrate human mucus.* J Control Release, 2013. **170**(2): p. 279-86.

154. Ishihara, T., et al., *Role of zinc in formulation of PLGA/PLA nanoparticles encapsulating betamethasone phosphate and its release profile.* J Control Release, 2005. **105**(1-2): p. 68-76.

155. Ishihara, T., et al., *Efficient encapsulation of a water-soluble corticosteroid in biodegradable nanoparticles.* Int J Pharm, 2009. **365**(1-2): p. 200-5.

156. Pan, Q., et al., *Corticosteroid-loaded biodegradable nanoparticles for prevention of corneal allograft rejection in rats.* J Control Release, 2015. **201**: p. 32-40.

157. Brock, T.A., et al., *Angiotensin Increases Cytosolic Free Calcium in Cultured Vascular Smooth-Muscle Cells.* Hypertension, 1985. **7**(3): p. I105-I109.

158. Pepperell, J.R., et al., *The Type-1 Angiotensin-Ii Receptor Mediates Intracellular Calcium Mobilization in Rat Luteal Cells.* Endocrinology, 1993. **133**(4): p. 1678-1684.

159. Roberts, C.J., et al., *Transforming growth factor beta stimulates the expression of fibronectin and of both subunits of the human fibronectin receptor by cultured human lung fibroblasts.* J Biol Chem, 1988. **263**(10): p. 4586-92.

160. Ignotz, R.A. and J. Massague, *Transforming growth factor-beta stimulates the expression of fibronectin and collagen and their incorporation into the extracellular matrix.* J Biol Chem, 1986. **261**(9): p. 4337-45.

161. Annoni, R., et al., *Extracellular matrix composition in COPD.* Eur Respir J, 2012. **40**(6): p. 1362-73.

162. Kuhn, C., 3rd, et al., *An immunohistochemical study of architectural remodeling and connective tissue synthesis in pulmonary fibrosis.* Am Rev Respir Dis, 1989. **140**(6): p. 1693-703.

163. Malmsten, M., *Block copolymers in pharmaceutics A2 - Alexandridis, Paschalis*, in *Amphiphilic Block Copolymers*, B. Lindman, Editor 2000, Elsevier Science B.V.: Amsterdam. p. 319-346.

164. Muller, R.H. and C. Jacobs, *Buparvaquone mucoadhesive nanosuspension: preparation, optimisation and long-term stability.* Int J Pharm, 2002. **237**(1-2): p. 151-61.

165. Hernandez-Trejo, N., et al., *Characterization of nebulized buparvaquone nanosuspensions--effect of nebulization technology.* J Drug Target, 2005. **13**(8-9): p. 499-507.

166. Shrewsbury, S.B., A.P. Bosco, and P.S. Uster, *Pharmacokinetics of a novel submicron budesonide dispersion for nebulized delivery in asthma.* Int J Pharm, 2009. **365**(1-2): p. 12-7.

167. Chiang, P.C., et al., *Pharmacokinetic and pharmacodynamic evaluation of the suitability of using fluticasone and an acute rat lung inflammation model to differentiate lung versus systemic efficacy.* J Pharm Sci, 2009. **98**(11): p. 4354-64.

168. Tang, B.C., et al., *Biodegradable polymer nanoparticles that rapidly penetrate the human mucus barrier.* Proc Natl Acad Sci U S A, 2009. **106**(46): p. 19268-73.

169. Mohanty, M.E., V.J. Rao, and A.K. Mishra, *A fluorescence study on the interaction of telmisartan in triblock polymers pluronic P123 and F127.* Spectrochim Acta A Mol Biomol Spectrosc, 2014. **121**: p. 330-8.

170. Zahr, A.S., C.A. Davis, and M.V. Pishko, *Macrophage uptake of core-shell nanoparticles surface modified with poly(ethylene glycol).* Langmuir, 2006. **22**(19): p. 8178-85.

171. Bazile, D., et al., *Stealth Me.PEG-PLA nanoparticles avoid uptake by the mononuclear phagocytes system.* J Pharm Sci, 1995. **84**(4): p. 493-8.

172. Besheer, A., et al., *Characterization of PLGA nanospheres stabilized with amphiphilic polymers: hydrophobically modified hydroxyethyl starch vs pluronics.* Mol Pharm, 2009. **6**(2): p. 407-15.

173. Yallapu, M.M., et al., *Multi-functional magnetic nanoparticles for magnetic resonance imaging and cancer therapy.* Biomaterials, 2011. **32**(7): p. 1890-905.

174. Yang, M., et al., *Vaginal delivery of paclitaxel via nanoparticles with non-mucoadhesive surfaces suppresses cervical tumor growth.* Adv Healthc Mater, 2014. **3**(7): p. 1044-52.

175. Elgogary, A., et al., *Combination therapy with BPTES nanoparticles and metformin targets the metabolic heterogeneity of pancreatic cancer.* Proc Natl Acad Sci U S A, 2016. **113**(36): p. E5328-36.

176. Tang, B.C., et al., *Enhanced efficacy of local etoposide delivery by poly(ether-anhydride) particles against small cell lung cancer in vivo.* Biomaterials, 2010. **31**(2): p. 339-44.

177. Wienen, W., et al., *A review on telmisartan: A novel, long-acting angiotensin II-receptor antagonist.* Cardiovascular Drug Reviews, 2000. **18**(2): p. 127-156.

178. McGrath-Morrow, S., et al., *Impaired lung homeostasis in neonatal mice exposed to cigarette smoke.* Am J Respir Cell Mol Biol, 2008. **38**(4): p. 393-400.

179. Wang, R.D., J.L. Wright, and A. Churg, *Transforming growth factor-beta1 drives airway remodeling in cigarette smoke-exposed tracheal explants.* Am J Respir Cell Mol Biol, 2005. **33**(4): p. 387-93.

180. Gross, N.J., *Novel antiinflammatory therapies for COPD.* Chest, 2012. **142**(5): p. 1300-1307.

181. Barnes, P.J., *New anti-inflammatory targets for chronic obstructive pulmonary disease.* Nat Rev Drug Discov, 2013. **12**(7): p. 543-59.

182. Ohnishi, S. and N. Nagaya, *Tissue regeneration as next-generation therapy for COPD--potential applications.* Int J Chron Obstruct Pulmon Dis, 2008. **3**(4): p. 509-14.

183. Lipsi, R., et al., *The clinical use of regenerative therapy in COPD.* Int J Chron Obstruct Pulmon Dis, 2014. **9**: p. 1389-96.

184. Oh, D.K., Y.S. Kim, and Y.M. Oh, *Lung Regeneration Therapy for Chronic Obstructive Pulmonary Disease.* Tuberc Respir Dis (Seoul), 2017. **80**(1): p. 1-10.

185. Perez-Rial, S., et al., *Liver growth factor treatment reverses emphysema previously established in a cigarette smoke exposure mouse model.* Am J Physiol Lung Cell Mol Physiol, 2014. **307**(9): p. L718-26.

186. Giron-Martinez, A., et al., *Proliferative activity of liver growth factor is associated with an improvement of cigarette smoke-induced emphysema in mice.* PLoS One, 2014. **9**(11): p. e112995.

187. Stessuk, T., et al., *Phase I clinical trial of cell therapy in patients with advanced chronic obstructive pulmonary disease: follow-up of up to 3 years.* Rev Bras Hematol Hemoter, 2013. **35**(5): p. 352-7.

188. Weiss, D.J., et al., *A placebo-controlled, randomized trial of mesenchymal stem cells in COPD.* Chest, 2013. **143**(6): p. 1590-1598.

189. Shiota, A., et al., *Telmisartan ameliorates insulin sensitivity by activating the AMPK/SIRT1 pathway in skeletal muscle of obese db/db mice.* Cardiovasc Diabetol, 2012. **11**: p. 139.

190. Okada, M., et al., *Effects of telmisartan on right ventricular remodeling induced by monocrotaline in rats.* J Pharmacol Sci, 2009. **111**(2): p. 193-200.

191. Cynis, H., et al., *Inhibition of Glutaminyl Cyclases alleviates CCL2-mediated inflammation of non-alcoholic fatty liver disease in mice.* Int J Exp Pathol, 2013. **94**(3): p. 217-25.

192. Garrido-Gil, P., et al., *Involvement of PPAR-gamma in the neuroprotective and anti-inflammatory effects of angiotensin type 1 receptor inhibition: effects of the receptor antagonist telmisartan and receptor deletion in a mouse MPTP model of Parkinson's disease.* J Neuroinflammation, 2012. **9**: p. 38.

193. Li, Y., et al., *Telmisartan attenuates the inflamed mesenteric adipose tissue in spontaneous colitis by mechanisms involving regulation of neurotensin/microRNA-155 pathway.* Biochem Pharmacol, 2015. **93**(4): p. 461-9.

194. Washida, K., et al., *Nonhypotensive dose of telmisartan attenuates cognitive impairment partially due to peroxisome proliferator-activated receptor-gamma activation in mice with chronic cerebral hypoperfusion.* Stroke, 2010. **41**(8): p. 1798-806.

195. Liu, R.M. and K.A. Gaston Pravia, *Oxidative stress and glutathione in TGF-beta-mediated fibrogenesis.* Free Radic Biol Med, 2010. **48**(1): p. 1-15.

196. Kitamura, H., et al., *Mouse and human lung fibroblasts regulate dendritic cell trafficking, airway inflammation, and fibrosis through integrin alphavbeta8-mediated activation of TGF-beta.* J Clin Invest, 2011. **121**(7): p. 2863-75.

197. Calvi, C., et al., *Hepatocyte growth factor, a determinant of airspace homeostasis in the murine lung.* PLoS Genet, 2013. **9**(2): p. e1003228.

198. Long, K.B., C.M. Artlett, and E.P. Blankenhorn, *Tight skin 2 mice exhibit a novel time line of events leading to increased extracellular matrix deposition and dermal fibrosis.* Matrix Biol, 2014. **38**: p. 91-100.

199. Lemaire, R., et al., *Antagonistic effect of the matricellular signaling protein CCN3 on TGF-beta- and Wnt-mediated fibrillinogenesis in systemic sclerosis and Marfan syndrome.* J Invest Dermatol, 2010. **130**(6): p. 1514-23.

200. Lemaire, R., J. Bayle, and R. Lafyatis, *Fibrillin in Marfan syndrome and tight skin mice provides new insights into transforming growth factor-beta regulation and systemic sclerosis.* Curr Opin Rheumatol, 2006. **18**(6): p. 582-7.

## Curriculum Vitae


### Jane Chisholm

1415 Jackson St Baltimore, MD 21230 | jchisho3@jhu.edu | 216-513-9776


### EDUCATION

**Johns Hopkins University, Baltimore, MD** 2010 – 2017

Ph.D. in Chemical & Biomolecular Engineering (expected)

**Johns Hopkins University, Baltimore, MD** 2005 – 2009

B.S. in Chemical & Biomolecular Engineering (graduated with honors)

### RESEARCH EXPERIENCE

**Johns Hopkins University, Baltimore, MD**

*Ph.D. Candidate* 2010 – 2017

- Engineered drug nanocrystals for the treatment of COPD and evaluated the efficacy in mouse models of COPD
- Characterized biophysical properties of COPD sputum via nanoparticle diffusion as a tool to probe disease severity in COPD
- Investigated the behavior of model mucus-penetrating nanoparticles following inhalation in mouse lungs
- Formulated, characterized and investigated the in vivo efficacy of chemotherapy loaded biodegradable nanoparticles for the local treatment of lung cancer
- Established and maintained long term collaborations with professors in Pulmonary and Critical Care Medicine and Johns Hopkins School of Medicine

*Master's Candidate* 2009 – 2010

- Engineered cell-adhesive mucus penetrating nanoparticles for lung cancer therapy
- Formulated and characterized chemotherapy loaded biodegradable nanoparticles

*Undergraduate Research Assistant* 2008 – 2009

- PEGylated polystyrene nanoparticles and tested their ability to diffuse in mucus secretions
- Formulated and characterized chemotherapy loaded biodegradable nanoparticles

**Color Matrix, Berea, OH** Summer 2008

*Research & Development Intern*

- Assisted in the development and testing of oxygen barrier technologies for PET bottles
- Developed test methods to determine pigment transfer in roto-molded parts

**Case Western Reserve University, Cleveland, OH** 2004 – 2005

*Research Assistant*

- Acquired basic lab skills and knowledge specific to fuel cell research
- Modified Nafion® based membranes to improve the efficiency of a direct methanol fuel cell

## LEADERSHIP AND TEACHING EXPERIENCE

**Cystic Fibrosis Foundation Great Strides Walk, Baltimore, MD**

*Team member and fundraiser* 2009 – 2017

- Helped raise donations and organize fundraising events
- Participated in the walk event

**Graduate Women's Empowerment Network at Johns Hopkins University, Baltimore, MD**

*Founding member and board member* 2014 – 2016

- Mission is to create a network of STEM doctoral students at Johns Hopkins University and increase the representation of doctoral women at all levels of STEM professions, especially those seeking leadership positions
- Organized Women in Science and Engineering (WISE) Words round table discussions with local women in STEM professions

**Center for Nanomedicine at Johns Hopkins University, Baltimore, MD**

*Mentor and Coordinator* 2011 – present

- Trained and mentored new graduate students, undergraduate research assistants, and visiting fellows
- Supervised and mentored local high school students in the summer
- Managed responsibilities within the center, enforced proper procedures, and established standard procedures

**Johns Hopkins University Center for Educational Resources, Baltimore, MD**

*Instructor, "Leading Labs: Engineering"* 2011 – 2012

- Designed and led an instructional course for new graduate student teaching assistants

**Thread, Non-profit organization Baltimore, MD**
*Head and Grandparent of Household* 2010 – 2016

- Strategized and coordinated efforts of 15+ Hopkins affiliated mentors to ensure academic success of at risk, underprivileged Baltimore City students
- Managed the after school tutoring program once a week

**Johns Hopkins University Chemical & Biomolecular Engineering Department, Baltimore, MD**
*Teaching assistant: Undergraduate Senior Laboratory* 2011

- Led students in operating distillation, biocatalysis, gas chromatography, and membrane extraction experiments
- Graded lab reports and prepared reagents

## HONORS AND AWARDS

1st place poster, European Symposium on Controlled Drug Delivery, 2016
Egmond aan Zee, The Netherlands.

200

Center for Nanomedicine Award for Research Excellence, 2014
Johns Hopkins University, Baltimore MD

Best poster award and selected for an oral presentation, NanoDDS 2014
University of North Carolina, Chapel Hill, NC

3rd place poster award, Johns Hopkins INBT annual symposium, 2013

Baltimore, MD

Whiting School of Engineering Dean's list, Johns Hopkins University 2005-2009
Baltimore, MD

## PUBLICATIONS

**Chisholm J,** Shade J, Dikeman D, Malinina A, Bandeira E, Roig Pons M, Shimoda L, Hanes J*, Neptune E*, Suk JS*. *Inhaled angiotensin receptor blocker nanoparticles for the treatment of COPD lung injury*. Manuscript in preparation.

Schneider C*, **Chisholm J***, Peacock C, and Hanes J. Cisplatin nanocomplexes for the local treatment of lung cancer. Manuscript in preparation.

**Chisholm J**, Suk JS, Shade J, Hansel N, Neptune E*, and Hanes J*. Nanoparticle diffusion in spontaneously expectorated sputum as a biophysical tool to probe disease severity in COPD. Manuscript in submission.

Huang H, **Chisholm J**, Zhuang J, Xiao Y, Duncan G, Chen X, Suk JS[#], Hanes J[#]. Protein nanocages that penetrate airway mucus and tumor tissue. PNAS. (2017).

Schneider C*, Xu Q*, Boylan N*, **Chisholm J**, Tang BC, Schuster BS, Henning A, Ensign LM, Lee E, Adstamongkonkul P, Simons BW, Wang SS, Gong X, Yu T, Boyle MP, Suk JS, Hanes J. Nanoparticles that do not adhere to mucus provide uniform and long-lasting drug delivery to airways following inhalation. Science Advances. 3, e1601556 (2017).

Zhang C, Nance E, Mastorakos P, **Chisholm J**, Berry S, Eberhart C, Tyler B, Brem H, Suk J, Hanes J. Convection enhanced delivery of cisplatin-loaded brain penetrating nanoparticles cure malignant glioma in rats. J Control Release. (2017).

Yu T, **Chisholm J**, Choi WJ, Anonuevo A, Pulicare S, Zhong W, Chen M, Fridley C, Lai SK, Ensign LM, Suk JS, Hanes J. Mucus-penetrating nanosuspensions for enhanced delivery of poorly soluble drugs to mucosal surfaces. Advanced Healthcare Materials. 5, 2745-2750 (2016).

Mastorakos P*, da Silva AL*, **Chisholm J**, Song E, Choi WK, Boyle MP, Morales MM, Hanes J[#], Suk JS[#]. Highly compacted biodegradable DNA nanoparticles capable of overcoming the mucus barrier for inhaled lung gene therapy. PNAS, 112, 8720-8725 (2015).

Wycisk R, **Chisholm J**, Lee J, Lin J, and Pintauro PN. Direct methanol fuel cell membranes from nafion-polybenzimidazole blends. Journal of Power Sources, 163, 9-17 (2006).

## CONFERENCE ABSTRACTS AND PRESENTATIONS

**Chisholm J**, Shade J, Suk JS, Neptune E, Hanes J. Lung targeting of angiotensin receptor blockers for treatment of COPD lung injury. *The European Symposium on Controlled Drug Delivery (ESCDD), Egmond aan Zee, The Netherlands, 2016.* (Poster presentation)

**Chisholm J**, Shade J, Suk JS, Neptune E, and Hanes J. Lung targeting of angiotensin receptor blockers for treatment of COPD lung injury. The 13th Annual International NanoDDS, Seattle, WA, 2015. (Poster presentation)

**Chisholm J**, Mastorakos P, da Silva A, Zhang C, Berry S, Choi P, Park HW, Hanes J, Suk JS. Highly compacted biodegradable DNA nanoparticles capable of overcoming extracellular barriers. *The Biomedical Engineering Society Annual Meeting, San Antonio TX, 2014.* (Poster presentation)

**Chisholm J**, Schneider C, Peacock C, Hanes J. Mucus-penetrating particles for the local treatment of lung cancer. *The 12th Annual International Nanomedicine & Drug Delivery Symposium (NanoDDS), Chapel Hill, NC, 2014.* (Poster Presentation)

**Chisholm J**, Schneider C, Peacock C, Hanes J. Mucus-penetrating particles for the local treatment of lung cancer. *The Johns Hopkins INBT Annual Symposium, Baltimore, MD, 2014*. (Poster presentation)

**Chisholm J**, Schneider C, Peacock C, Hanes J. Mucus-penetrating particles for the local treatment of lung cancer. *National Cancer Institute site visit of the Johns Hopkins University CCNE, Baltimore, MD, 2014.* (Poster presentation)

**Chisholm J**. Mucus-penetrating particles for the local treatment of lung cancer. *Johns Hopkins University CCNE meeting, Baltimore, MD, 2013*. (Podium presentation)

**Chisholm J**, Wise R, Hansel N, Hanes J, Neptune E. Nanoparticle diffusion in sputum as a biomarker of COPD severity. *The Annual Meeting of the American Thoracic Society, Philadelphia, PA, 2013.* (Poster presentation)

**Chisholm J**, Schneider C, Peacock C, Hanes J. Mucus-penetrating cisplatin nanoparticles for the local treatment of lung cancer. *The Johns Hopkins INBT annual symposium, Baltimore, MD, 2013.* (Poster presentation)

**Chisholm J**, Schneider C, Peacock C, Hanes J. Mucus-penetrating cisplatin nanoparticles for the local treatment of lung cancer. *National Cancer Institute site visit of the Johns Hopkins University Center of Cancer Nanotechnology (CCNE), Baltimore, MD, 2013.* (Poster presentation)

**Chisholm J**. Cisplatin nanoparticles for the local treatment of lung cancer. *Johns Hopkins Center for Cancer Nanotechnology Excellence and Physical Science Oncology Center Symposium, Baltimore, MD, 2012.* (Invited podium talk)

**Chisholm J**, Schneider C, Peacock C, Hanes J. Mucus-penetrating cisplatin nanoparticles for the local treatment of lung cancer. *The Johns Hopkins INBT annual symposium, Baltimore, MD, 2012.* (Poster presentation)

**Chisholm J**, Tang B, Dawson M, Lai S, Wang YY, Yang M, Fu J, Peacock C, Hanes J. Mucus penetration biodegradable nanoparticles for the local delivery of chemotherapeutics to lung cancer. *Johns Hopkins Institute for NanoBioTechnology (INBT) annual symposium, Baltimore, MD, 2011.* (Poster presentation)